LBL-13768
Reprint

Lawrence Berkeley Laboratory
UNIVERSITY OF CALIFORNIA

DOCUMENTS SECTION

Published in Physical Review C, Volume 27, No. 2,
February 1983, pp. 606-627

MONTE CARLO STUDIES OF PION DISTRIBUTIONS
FROM HEAVY ION COLLISIONS

Hafez M.A. Radi, John O. Rasmussen,
Kenneth A. Frankel, John P. Sullivan, and
H.C. Song

December 1982

NUCLEAR SCIENCE DIVISION

Prepared for the U.S. Department of Energy under Contract DE-AC03-76SF00098

LBL-13768

DISCLAIMER

This document was prepared as an account of work sponsored by the United States Government. While this document is believed to contain correct information, neither the United States Government nor any agency thereof, nor the Regents of the University of California, nor any of their employees, makes any warranty, express or implied, or assumes any legal responsibility for the accuracy, completeness, or usefulness of any information, apparatus, product, or process disclosed, or represents that its use would not infringe privately owned rights. Reference herein to any specific commercial product, process, or service by its trade name, trademark, manufacturer, or otherwise, does not necessarily constitute or imply its endorsement, recommendation, or favoring by the United States Government or any agency thereof, or the Regents of the University of California. The views and opinions of authors expressed herein do not necessarily state or reflect those of the United States Government or any agency thereof or the Regents of the University of California.

Monte Carlo studies of pion distributions from heavy ion collisions

Hafez M. A. Radi
Nuclear Science Division, Lawrence Berkeley Laboratory, University of California, Berkeley, California 94720 and Physics Department, Kuwait University, Kuwait

John O. Rasmussen, Kenneth A. Frankel, and John P. Sullivan*
Nuclear Science Division, Lawrence Berkeley Laboratory, University of California, Berkeley, California 94720

H. C. Song
Nuclear Physics Research Institute, Academia Sinica, Shanghai, People's Republic of China
(Received 26 January 1982)

The Coulomb effects on slow pions formed in heavy ion collisions are investigated here by Monte Carlo methods. The trajectory calculations differ from some earlier theoretical work in that pions are considered to be absorbed if they pass within 0.8 radius of a spectator nuclear center. Absorption in the fireball is implicit in the treatment. The source function (i.e., π^0 cross section without shadowing) is also more detailed in that we use a linear combination of thermalized and unthermalized terms based on two-fireball and row-on-row models. The numerical calculations are mainly applied to the system ^{20}Ne+^{20}Ne at $E/A=655$ MeV and resulting π^-/π^+ ratios and spectra are in satisfactory agreement with experimental results for ^{20}Ne+NaF at this energy.

NUCLEAR REACTIONS Theory of Coulomb distortion of pion spectra by heavy-ion reactions. ^{20}Ne(NaF,$\pi^{\pm}$)X, $E/A=655$ MeV, ^{40}Ar(^{40}Ca,$\pi^{\pm}$)X, $E/A=1.05$ GeV, Monte Carlo trajectories, row-on-row model, thermalized and nonthermalized (nascent) pions, π^-/π^+ ratio.

I. INTRODUCTION

Now after several studies on pion production in heavy ion collisions the general features have been established and qualitatively understood. For example, the measurements of the Coulomb effects on the π^-/π^+ ratio demonstrated by Benenson *et al.*[1] have been investigated by Libbrecht and Koonin,[2] Cugnon and Koonin,[3] and Gyulassy and Kauffmann.[4] In these theoretical studies the pion trajectories were allowed, explicitly or implicitly, to propagate through nuclear matter. Further study of the Coulomb effects was made by Bertsch[5] in explaining the dependence of the π^-/π^+ ratio on the incident bombarding energy. Radi *et al.*[6] formulated the Coulomb effects of spectator fragments on the pion production cross sections near beam velocity in terms of weighted average over various projectile fragments.

In the work of Cugnon and Koonin,[3] the ability of low-energy charged pion spectra to probe the space-time evolution of high-energy nucleus-nucleus collisions is investigated in a classical picture. For pions emitted in both a thermal and direct process they calculate the electromagnetic distortion due to the time-dependent nuclear charge distribution by solving classical equations of motion. In Ref. 4 various approximate analytical expressions were derived for thermally expanding charge distributions. These theoretical expressions are based on unbound, free-gas expansion of the spectator and fireball charge distributions with their characteristic temperatures.

Here we shall be mainly concerned with the Coulomb effects on pions that are slower than beam and projectile in the center-of-mass (c.m.) frame. Frankel *et al.*[7] in reporting experimental results for ^{40}Ar on calcium at E/A of 1.05 GeV showed significantly lower π^-/π^+ ratios around zero velocity (c.m.) than were predicted in earlier theoretical studies. The Monte Carlo trajectory calculation of Koonin and Cugnon[3] gave a central ratio of 5.5, whereas experiment gave 1.5. More recently, new measurements[8] of the doubly differential cross section for the production of π^- and π^+ from c.m. to beam velocity for Ne on NaF at E/A of 655 MeV became available. In the present paper we mostly carry out theoretical calculations for the latter system.

 ©1983 The American Physical Society

In view of disagreements on π^-/π^+ ratios near rest in the center of mass, we decided to carry out new Monte Carlo pion trajectory calculations. We wished especially to test the effects of not allowing pions to propagate through nuclear matter. It is clear that results will be affected by the dependence of pion production on the impact parameter. Thus, we carry out the final weighting over impact parameter using a row-on-row, two-fireball model with thermal but not chemical equilibrium between pions and nucleons. A nonthermalized (nascent) pion source term is also included. For our Monte Carlo calculations the very complex situation had to be reduced to a practical model. Principal differences we wished to test relative to the Cugnon and Koonin work[3] were the following: (1) The pions should originate from the surface, not throughout the collision volume; (2) those trajectories that passed through nuclear matter should be rejected due to pion reabsorption; (3) the pions should be emitted at the time of closest approach, not the late stage of the collision; and (4) a two-fireball thermal plus first-collision source for initial pion momentum distribution was taken, rather than a single thermal source.

II. THE HEAVY ION REACTION MODEL

We develop here a model for investigation of the Coulomb effect on pions produced in heavy ion reactions. The collision problem is very complex, so one must greatly simplify the problem while retaining the essential features. The model presented here contains rough approximations, but we believe that it describes the main features of slow pion production by heavy ion reactions for the delta-production threshold region at 0.5 GeV $\lesssim E/A \lesssim$ 1.0 GeV. Further refinements to the model can be made without altering the qualitative results. Before launching into the description of the model, however, let us take care of some preliminaries.

A. General description

To develop a model for initial conditions of trajectories we view the collision of two spherical nuclei, at a given impact parameter, originally filled with cold nucleons as shown in the schematic representation of part (a) of Fig. 1. The process is viewed in the center of mass coordinate system. In part (a) A_P^0 and Z_P^0 are the mass number and atomic number of the projectile (likewise A_T^0 and Z_T^0 are for the target). The projectile and target are moving with center-of-mass velocities $\vec{V}_P^0$ and $\vec{V}_T^0$, respectively, in the x direction. One can at this point calculate the velocity of the center-of-mass system in the laboratory in units of c (the target has zero velocity in the laboratory) as

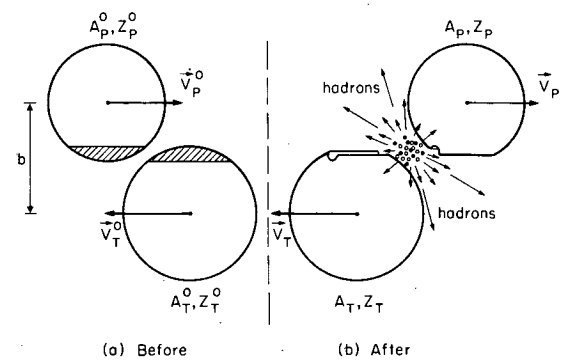

FIG. 1. Schematic diagram of the heavy ion collision with designation of parameters (c.m.).

$$\beta_{\text{c.m.}} = \frac{P_{\text{lab}}}{E_{\text{lab}}} = \frac{[1+2(m_N c^2/\epsilon_k)]^{1/2}}{1+(A_P^0+A_T^0)m_N c^2/(A_P^0\epsilon_k)} , \tag{1}$$

where P_{lab} is the total momentum of the system in the laboratory, E_{lab} is the total energy (kinetic plus mass) of the system, ϵ_k is the beam kinetic energy per nucleon, and $m_N c^2$ is the effective nucleon rest mass in nuclei (the mass of a bound nucleon $\simeq$931 MeV).

Before the collision takes place the density of cold nucleons, ρ_0, is uniform within the two nuclei. As the reaction proceeds, the two nuclei will scrape each other, shearing away all nucleons located within the geometrical overlap region (participant nucleons or the so-called fireball) as shown in part (b) of Fig. 1. Since the energy of the collision is very high, the projectile fragment (A_P,Z_P) will fly off after the collision with essentially unchanged velocity ($\vec{V}_P \simeq \vec{V}_P^0$ in c.m.) (a spectator in this collision). Similarly, the same arguments will apply to the target nucleus. Experimental confirmation of projectilelike spectators is available in Ref. 9 and spread in velocities can be related to the Fermi motion of the nucleons.[10] These fragments[11] (spectators) will usually evaporate nucleons, but their temperatures are too low to produce pions. Constituents of the hot hadronic matter are presumed to interact a few times before disassembly in heavy ion collision. In the early stage of the collision the energy concentration is enough (compressed nuclear matter) to produce pions and resonances. At this stage, different sorts of hadrons coexist, but the degree of chemical equilibrium or thermal equilibrium is an open question. As time goes on, this fireball begins to expand, and when it has reached some final volume V, it becomes a system of noninteracting expanding had-

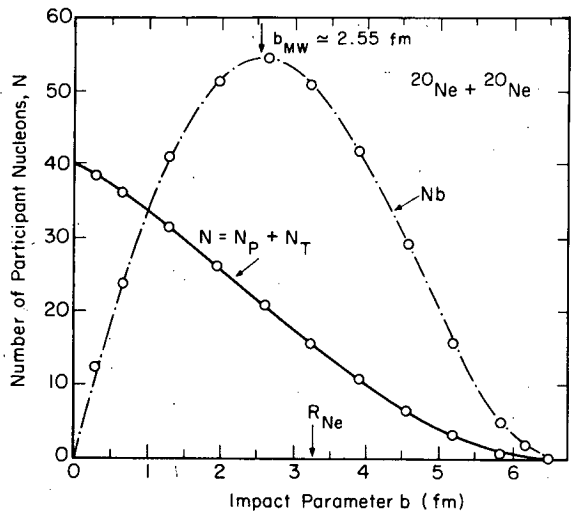

FIG. 2. For $^{20}Ne+{}^{20}Ne$ collisions in the abrasion ablation model the number of participant nucleons N (solid line) and the relative weight function N times impact parameter b (dashed-dotted line) are plotted. The abscissa is the impact parameter in fm.

rons.[12] At a given impact parameter b, the numbers of projectile, N_P, and target, N_T , participant nucleons can be computed by analytical approximation formulas given by Ref. 13. Figure 2 shows the variation of this number, $N=N_P+N_T$, as a function of the impact parameter b (as well as the product Nb). It is a good approximation to assume that this number does not depend on the bombarding energy.

B. Space-time history of the pion-emitting region

In this section we give the general assumptions for the starting point of the pion trajectory. First let us consider the distribution of matter between the projectile and target when the two spheres begin to overlap. Figure 3 is a schematic two-dimensional representation to illustrate how the nuclear density distributions are expected to develop with time. In part (a) of the figure the material in the overlap region starts into the compression regime, while some nucleons from the outer surface start to fly away. Part (b) of the figure shows the situation at the maximum overlap for this impact parameter and, we assume, the greatest probability for the appearance of pions at the surface. In part (c) the disassembly process of the fireball is in progress. The question of the time at which to start pion trajectories is not simple. Cugnon and Koonin[3] assumed a fairly late time after most nucleon collisions were over. We have taken the instant of closest approach as our time zero, since it is uniquely defined, but this time would be strictly justified only if the pion equilibration time were much shorter than the nuclear transit time. Another task is to specify a pion initial distribution in phase space with respect to the center of mass of the fireball. We use a more complex prescription than a simple thermal source but relegate these details to the appendixes. Then a Monte Carlo random selection of initial position and momentum is made, and we run the classical trajectory of the π^+, π^-, and π^0 in the field of moving spectator point charges. The complexities of finite charge distributions are unnecessary, since any trajectory passing inside $0.8R_{\text{spect}}$ of a spectator fragment center is stopped and recorded as a reabsorbed pion. In principle, one should take into account hadronic scattering as well as true absorption, but that is a complication avoided here as in the previous Monte Carlo studies.

What about the effect of the hot expanding participant protons? As we shall amplify in the later section on determination of the classical Jacobian, the Coulomb effects of participant protons on the slow-pion cross sections should be small and will be factored in for the center of mass region using expressions derived near the end of this paper. Having decided in the Monte Carlo calculations to treat spectators as two point-charges moving with essentially unchanged velocities and to neglect participant

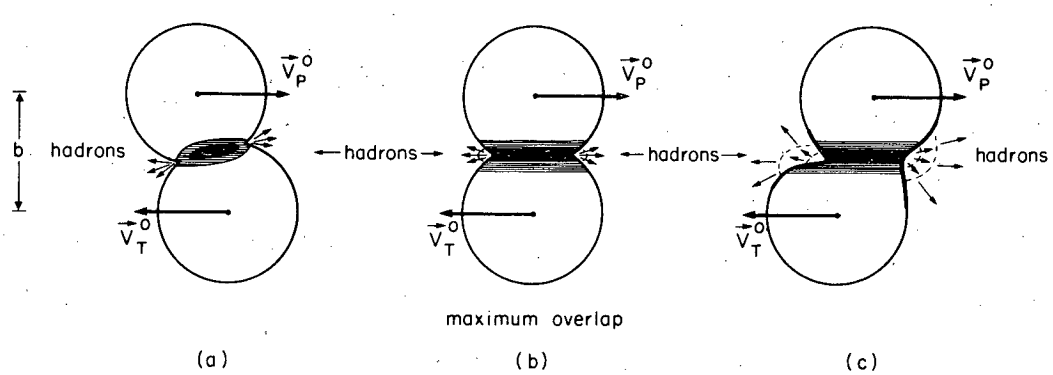

FIG. 3. Schematic sketches of the heavy ion collision and pion production for three successive times (c.m.).

charge effects at the end, we next must decide about the appropriate initial spatial positions. For pions we choose to start all pion trajectories from the ring at the intersection of the surfaces of the projectile and target at closest approach [part (b) of Fig. 3].

Let us next consider the geometry of the system at maximum overlap. In the spirit of the one-fireball[12] or two-fireball[14–16] and firestreak[17,18] models the projectile and target are assumed to make clean cylindrical cuts through each other, leaving projectile and target spectator residues (spectators).

The charge of the spectators is found from

$$Z_i(b)=Z_i^0-\left[\frac{Z_i^0}{A_i^0}\right]N_i(b) \quad (i=P,T)\ , \tag{2}$$

where these variables were already defined in Sec. II A. The spectator mass numbers $A_i(b)$ $(i=P,T)$ are also found from a formula similar to Eq. (2). Once we remove the participant nucleons we end up with peculiar nuclear shapes. Also the center of mass of each spectator has been shifted away from the region of maximum overlap. In Appendix A the shift, δb, of the center of mass of the spectators with respect to the original centers is approximately formulated. Then the distance between the new centers is obtained by (see Fig. 20)

$$D=b+\delta b_P+\delta b_T\ . \tag{3}$$

If we assume the spectators to resume spherical shapes about the new centroids, then the new radii for the spectators become

$$R_i(b)=r_0[A_i^0-N_i(b)]^{1/3}\ ,$$
$$\text{with } r_0=1.2 \text{ fm}\ . \tag{4}$$

After making these approximations, the geometry of the model and the ring from which pions originate appear as shown schematically in Fig. 4. In this figure Cartesian coordinates (xyz) are given with respect to the center of mass of the projectile spectator, the target spectator, and the pion. One should notice that the velocity of the projectile and target are no longer $\vec{V}_P^0$ and $\vec{V}_T^0$. The slight change is incorporated to constrain the total momentum to zero in the c.m. frame. In heavy ion reactions at the low charge and high energy treated here, this modification has almost no effect on the projectile and target center of mass velocity, but our program was developed to give exact nonrelativistic three-body solutions including recoil and all Coulomb effects among three bodies.

C. The initial starting point in phase space

In this subsection we would like to present the equations of the initial positions and velocities of the

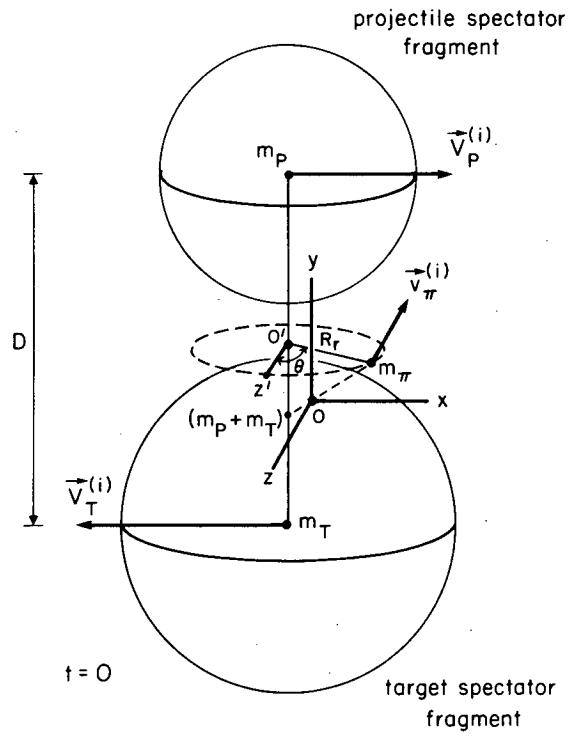

FIG. 4. Sketch defining coordinates and variables for pion initial conditions at time $t=0$ with respect to the center of mass frame attached at 0.

spectators and pion at $t=0$ (the time of closest approach). We randomly choose the pion position on the surface intersection ring at the angle θ_π between 0 and $\pi/2$ (as shown in Fig. 4). The components of the pion velocity along x, y, and z are chosen at random (positive as well as negative) from a flat distribution (we later introduce a row-on-row two-fireball model weighting function to the final results) as

$$v^{(i)}=(2\xi-1)V_{\text{lim}}\ , \tag{5}$$

where ξ is a random number between 0 and 1 and V_{lim} is the absolute value of the maximum velocity component to be chosen. The initial positions and velocities of the projectile, target, and pion viewed from the center of mass are generally written as

$$\vec{r}_j^{(i)}=x_j^{(i)}\hat{e}_x+y_j^{(i)}\hat{e}_y+z_j^{(i)}\hat{e}_z\ , \tag{6}$$

$$\vec{v}_j^{(i)}=v_{xj}^{(i)}\hat{e}_x+v_{yj}^{(i)}\hat{e}_y+v_{zj}^{(i)}\hat{e}_z\ ,\quad (j=P,T,\pi)\ . \tag{7}$$

The components of these two equations are presented in Table I. It is clear that for a given impact parameter a random choice of θ_π will change $x_j^{(i)}$ and $z_j^{(i)}$ coordinates, leaving $y_j^{(i)}$ unchanged. In this table, the ring radius R_r and distance d are defined in Appendix A.

TABLE I. Initial coordinates and velocities of the projectile, target, and pion with respect to the c.m. M is the total mass of the system, m_{PT} is the total mass of the spectators, and m_i $(i=P,T,\pi)$ stands for the individual mass. $\delta Y=d-(m_T/m_{PT})D$. $\delta V=(m_P V_P^0-m_T V_T^0+m_\pi v^{(i)})/m_{PT}$. R_r and d are defined in Appendix A.

j	$x_j^{(i)}$	$y_j^{(i)}$	$z_j^{(i)}$
P	$-(m_\pi/M)R_r\sin\theta$	$m_\pi/M\delta Y+(m_T/m_{PT})D$	$-(m_\pi/M)R_r\cos\theta$
T	$x_P^{(i)}$	$-(m_{PT}/M)\delta Y-D+d$	$z_P^{(i)}$
π	$(m_{PT}/M)R_r\sin\theta$	$-(m_{PT}/M)\delta Y$	$(m_{PT}/M)R_r\cos\theta$
j	$v_{xj}^{(i)}$	$v_{yj}^{(i)}$	$v_{zj}^{(i)}$
P	$v_P^0-\delta V$	$-(m_\pi/m_{PT})v_{y\pi}^{(i)}$	$-(m_\pi/m_{PT})v_{z\pi}^{(i)}$
T	$v_T^0-\delta V$	$v_{yP}^{(i)}$	$v_{zP}^{(i)}$
π	$v_{x\pi}^{(i)}$	$v_{y\pi}^{(i)}$	$v_{z\pi}^{(i)}$

III. DYNAMICS OF THE MODEL

We shall be concerned in this section with the classical solution for the pion and two charged spectator fragments (the three-body problem). Figure 5 shows the motion of the two spectator fragments and the pion with respect to the center of mass at a given time t. This figure represents a later time than Fig. 4, which defined the initial conditions of the problem. The charges are to be considered as point charges, as mentioned before. With the use of variables defined in Fig. 5 we can write the requirement of having zero total momentum as

$$\sum_i m_i \dot{\vec{r}}_i=0\ , \quad (i=P,T,\pi) \tag{8}$$

where m_i, r_i, and t at this stage have the units of mass, distance, and time, respectively. The kinetic energy of the system about the c.m. is

$$E_K=\sum_i \tfrac{1}{2}m_i(\dot{\vec{r}}_i\cdot\dot{\vec{r}}_i)\ , \quad (i=P,T,\pi)\ . \tag{9}$$

The potential energy of the system is simply the Coulomb potential energy of the interacting three particles and is written as

$$V_{\text{pot}}=\sum_{\substack{i,j\\ i\neq j}} \frac{Z_iZ_je^2}{[(x_i-x_j)^2+(y_i-y_j)^2+(z_i-z_j)^2]^{1/2}}\ , \quad (i,j=P,T,\pi)\ . \tag{10}$$

The Lagrangian of the system can be constructed and used in Lagrange's equation to get the differential equations of motion. In general, we get differential equations for the projectile spectator, target spectator, and pion. One can use to advantage the conservation of momentum of the system to decouple, for instance, the target spectator fragment variables. This will allow us to solve the differential equation of the projectile spectator fragment and the pion only. As a result of this step, the coupled first-order differential equations of the projectile spectator fragment and the pion are

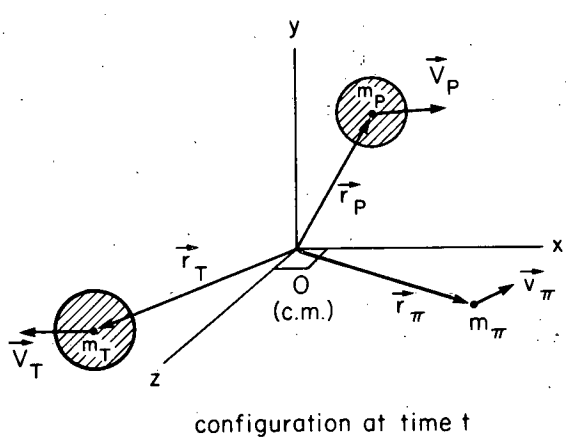

FIG. 5. Sketch defining coordinates during the evolution of the three-body trajectories at time t with respect to the center of mass attached at 0.

$$\frac{d\hat{x}_P}{d\hat{t}}=\hat{v}_{xP}\ ,$$
$$\frac{d\hat{v}_{xP}}{d\hat{t}}=\frac{Z_Pe^2}{m_Pc^2R_0\beta_0^2}[Z_\pi A_x/A+Z_TB_x/B]\ , \tag{11}$$

and similar equations for y and z,

$$\frac{d\hat{x}_\pi}{d\hat{t}}=\hat{v}_{x\pi}\ ,$$
$$\frac{d\hat{v}_{x\pi}}{d\hat{t}}=\frac{Z_\pi e^2}{m_\pi c^2 R_0 \beta_0{}^2}[-Z_P A_x/A+Z_T C_x/C]\ , \tag{12}$$

and similar equations for y and z, where

$$A_x=\hat{x}_P-\hat{x}_\pi \tag{13a}$$

and similar ones for A_y and A_z,

$$A=(A_x{}^2+A_y{}^2+A_z{}^2)^{3/2}\ , \tag{13b}$$

$$B_x=(1+m_P/m_T)\hat{x}_P+(m_\pi/m_T)\hat{x}_\pi \tag{14a}$$

and similar ones for B_y and B_z,

$$B=(B_x{}^2+B_y{}^2+B_z{}^2)^{3/2}\ , \tag{14b}$$

$$C_x=(m_P/m_T)\hat{x}_P+(1+m_\pi/m_T)\hat{x}_\pi \tag{15a}$$

and similar ones for C_y and C_z,

$$C=(C_x{}^2+C_y{}^2+C_z{}^2)^{3/2}\ , \tag{15b}$$

and where the dimensionless variables, $\hat{x}$, $\hat{v}$, $\hat{t}$, and β_0 are given by

$$\hat{x}=x/R_0\ ,$$
$$\hat{v}=v/V_0\ , \tag{16}$$
$$\hat{t}=t/T_0\ ,$$
$$\beta_0=V_0/c\ .$$

R_0 is taken to be the average of the radii of the spectator

$$R_0=(R_P+R_T)/2\ . \tag{17}$$

Also, V_0 is taken to be the average of the speed of the projectile and target before interaction, i.e.,

$$V_0=(V_P^0+V_T^0)/2\ . \tag{18}$$

Finally, T_0 is taken to be

$$T_0=R_0/V_0\ . \tag{19}$$

This system of coupled first-order differential equations is integrated using the modified Adams-Moulton predictor-corrector method. The integration is continued until the change in the pion velocity becomes $\leq 0.001\%$ per step, unless it is terminated by passage too near a spectator nucleus.

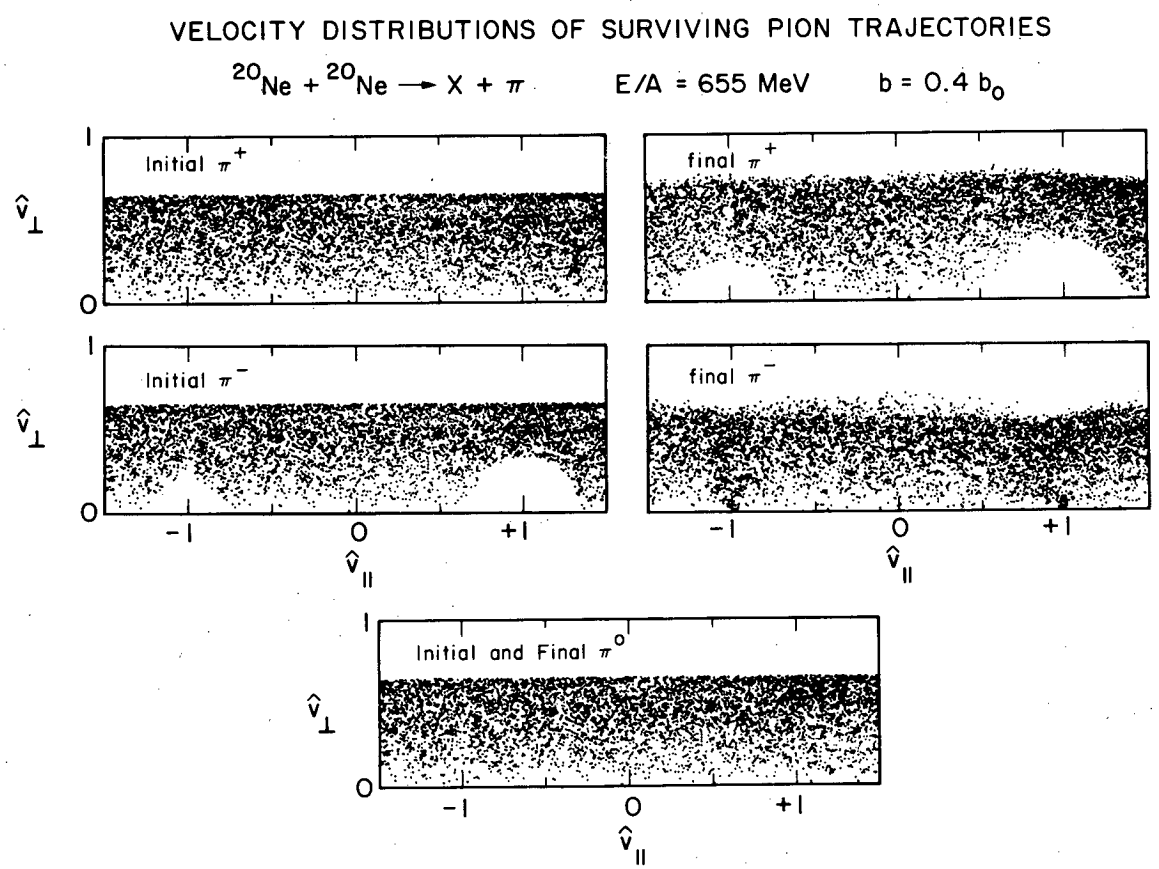

FIG. 6. Scatter plot of Monte Carlo initial and final $\hat{v}_\parallel$ and $\hat{v}_\perp$ values for trajectories surviving absorption or orbiting capture. Values are shown for one impact parameter $0.4b_0$ for the ^{20}Ne+^{20}Ne system at 655 MeV/nucleon (see text).

For an average value of the impact parameter ($b=0.4b_0$, $b_0=R_P^0+R_T^0$) for ^{20}Ne+^{20}Ne at $E/A=655$ MeV we show the results for about 10 000 surviving trajectories (for each type of pion). The scatter plots of Fig. 6 give initial and final velocity distributions for surviving trajectories of π^0, π^-, and π^+, with the abscissa $\hat{v}_{\parallel}\equiv(\hat{v}_x)$ and ordinate $\hat{v}_{\perp}\equiv[\hat{v}_y{}^2+\hat{v}_z{}^2]^{1/2}$. Note in the final distributions (upper right plots) the exclusion of π^+ from the velocity region near target and projectile, and note the bunching of π^- in these regions. The distributions are not symmetric in the sign of $\hat{v}_{\parallel}$, since the Monte Carlo selection of positions on the ring is only over the range $0\le\theta_\pi\le\pi/2$ with θ_π the angle with respect to the z axis (Fig. 4). Hence, the negative $\hat{v}_{\parallel}$ values are more susceptible to nuclear absorption (the trajectory falling within 0.8 of a spectator radius). Of course, the final averaged data must have the symmetry that is forced by identity of target and projectile. Hence, in the final weighted sums for pion cross sections, results are binned by the absolute value $|\hat{v}_{\parallel}|$. The complete exclusion of π^+ from the regions near target and projectile velocities is a consequence of the classical treatment, and a quantal treatment would bring some π^+ into the classically forbidden region. There is only one plot for π^0, since initial and final distributions are the same (for surviving trajectories). The π^0 distributions of surviving trajectories are of interest, since shadowing by spectator pieces removes some initial coordinate-velocity selections. It is not possible to display on a two-dimensional scatter plot the four randomly chosen variables (three velocity components and the angular position on the source ring), so the π^0 scatter plot is a projection of the four-dimensional initial distribution on the $\hat{v}_{\parallel}-\hat{v}_{\perp}$ plane. The upper left two plots are the analogous velocity-plane projections of the initial parameters for *surviving* trajectories of π^- and π^+. Large empty spaces are seen around the projectile and target velocity for π^- (the initial distribution). These holes define the regions of initial conditions leading to π^- absorption and to orbiting trajectories that never converge to a constant velocity. (For these low-Z systems we do not believe the orbiting trajectories correspond to pionic non-s state orbits,[19] since angular momenta are much less than $\hbar$.) For the π^+ initial-velocity scatter plot the least absorption effects of all are observed, since the repulsive Coulomb force acts to promote π^+ avoidance of the spectator nuclei.

IV. CLASSICAL JACOBIAN

In this section, a detailed study of the Coulomb effect on pions (with identical initial distributions for π^- and π^+) originating from the point of contact between the projectile and target is presented. Here we take only the grazing impact parameter, $b=b_0$. Generally, we start with

$$\left[\frac{d^6\sigma_i}{dP_i{}^3dr_i{}^3}\right]_{\pi^\pm}$$

initial distribution of pions from an infinitesimal, initial volume dP^3dr^3 in phase space. In order to map in momentum space from the initial to final conditions, one can write

$$\left[\frac{d^3\sigma_f}{dP_f{}^3}\right]_{\pi^\pm}=\int\left[\frac{d^6\sigma_i}{dP_i{}^3dr_i{}^3}\right]_{\pi^\pm}dr_i{}^3\left|\frac{\partial^3(\vec{P}_i)}{\partial^3(\vec{P}_f)}\right|_{\pi^\pm}. \tag{20}$$

In this equation, it is clear that the change in the density of the states (in momentum space) is expressed via the classical Jacobian

$$J_{\pi^\pm}=\left|\frac{\partial^3(\vec{P}_i)}{\partial^3(\vec{P}_f)}\right|_{\pi^\pm}.$$

By considering a simple case where the initial pion distributions are independent of spatial coordinates, Eq. (20) is simply written as

$$\left[\frac{d^3\sigma_f}{dP_f{}^3}\right]_{\pi^\pm}=J_{\pi^\pm}\left[\frac{d^3\sigma_i}{dP_i{}^3}\right]_{\pi^\pm}. \tag{21}$$

The ratio of negatively and positively charged pions is then

$$\left[\frac{d^3\sigma_f}{dP_f{}^3}\right]_{\pi^-}\Big/\left[\frac{d^3\sigma_f}{dP_f{}^3}\right]_{\pi^+}=J_{\pi^-}/J_{\pi^+}. \tag{22}$$

One can compute

$$\left|\frac{\partial^3(\vec{P}_f)}{\partial^3(\vec{P}_i)}\right|_{\pi^\pm}=\frac{1}{J_{\pi^\pm}}$$

numerically by the method of finite differences by mapping initial momenta $\vec{P}_i$ onto final momenta $\vec{P}_f$. Alternatively, one can compute an initial infinitesimal volume in momentum space about a momentum $\vec{P}_i$ and compute the corresponding final volume about $\vec{P}_f$ by mapping initial momenta to final momenta. The initial volume can be chosen to be the volume of eight tetrahedra as shown in Fig. 7. Each tetrahedron has a volume

$$\Delta V_{\text{init}}=\frac{1}{6}\begin{vmatrix} P_{x_1}-P_{x_i} & P_{y_1}-P_{y_i} & P_{z_1}-P_{z_i}\\ P_{x_2}-P_{x_i} & P_{y_2}-P_{y_i} & P_{z_2}-P_{z_i}\\ P_{x_3}-P_{x_i} & P_{y_3}-P_{y_i} & P_{z_3}-P_{z_i}\end{vmatrix}, \tag{23}$$

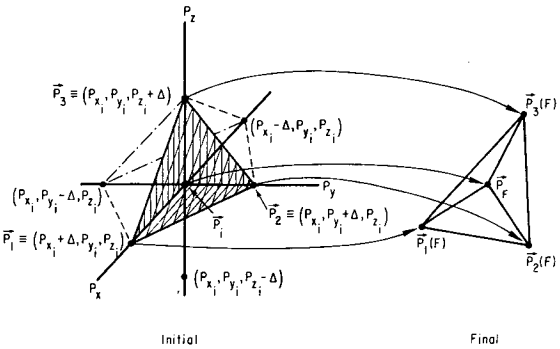

FIG. 7. Sketch illustrating the mapping of a tetrahedron in momentum space from initial to final conditions.

where $\vec{P}_i$, $\vec{P}_1$, $\vec{P}_2$, and $\vec{P}_3$ are the momenta determining the tetrahedron corners. Thus

$$J_{\pi^-}/J_{\pi^+}=\frac{\left\{\sum \Delta V^{\pi^-}_{\text{init}}\Big/\sum \Delta V^{\pi^-}_{\text{fin}}\right\}}{\left\{\sum \Delta V^{\pi^+}_{\text{init}}\Big/\sum \Delta V^{\pi^+}_{\text{fin}}\right\}} . \tag{24}$$

However, analytical evaluation of the Jacobian is possible only if one of the spectator fragments has a zero charge (i.e., in the absence of either the projectile or the target spectator fragments). Some elements of the Jacobian determinants can be found analytically from conservation of energy, while the others could be obtained from the analytical solution of a general Kepler problem. We have compared the analytic Jacobian to the numerical one by letting one of the spectator charges be zero (in the numerical code). This provides a useful estimate of the error in the numerical calculations. By such checks we noted occasional errors in the fourth significant figure between the analytical and numerical calculations, which is sufficient accuracy for this study. In Fig. 8 the velocity shift $\delta\hat{\vec{v}}=\hat{\vec{v}}_f-\hat{\vec{v}}_i$ is displayed (where $\hat{\vec{v}}$ is the pion velocity in units of V_0 as defined in the previous section) for $^{40}\text{Ar}+^{40}\text{Ca}$ at $E/A=1.05$ GeV, $V_0=0.6c$. In the same figure, the π^-/π^+ ratios computed from Eq. (24), as well as computed from Eqs. (2.7) and (2.8) of Ref. 4, are displayed.

One sees the π^- velocities are systematically shifted (solid line) toward the projectile (Fig. 4) that is closest in velocity space for positive $V_y^{(i)}$, and the π^+ (dashed line) are shifted away. The ratio of the Jacobians for π^- and π^+ is shown at the end of the arrow. These Jacobians were calculated from the volume change of tetrahedra of six close-lying points in velocity space. The values agree with results using the conventional 3×3 determinantal form. The approximate form of Ref. 4, relating the Jacobian to the divergence of the velocity shift field $J_\pm=1\mp\nabla\cdot\delta\hat{\vec{v}}$, was used to calculate the values displayed in italics. These values are not in agreement, perhaps because the formula is based on a common origin expanding charges and on divergence of the velocity shift, which is only a perturbative approximation. Further, our numerical studies on the Jacobian show that for the slow pion starting from the midpoint of two equal spectator charges of opposite velocities, there is an almost complete cancellation of Coulomb effects, leaving the Jacobians near unity.

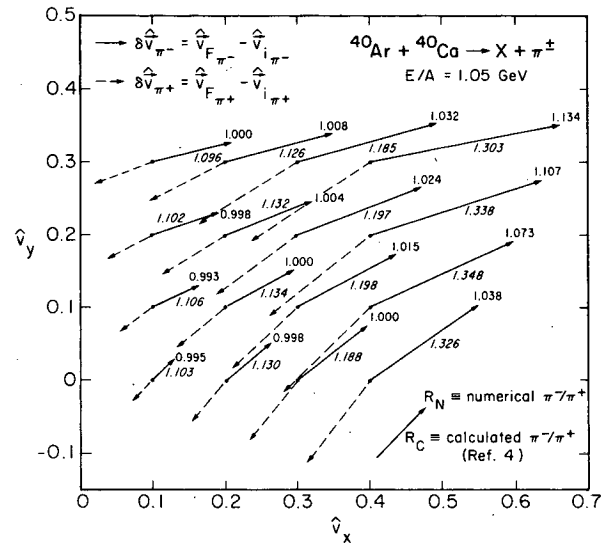

FIG. 8. Map of velocity shift (for pions with $\hat{\vec{v}}_z=0$) fields (c.m. frame) for grazing impact parameter for π^- (solid arrows) and π^+ (dashed arrows). The position of the ^{40}Ar nucleus is in the positive y direction with its velocity directed along the positive x axis. The Roman numbers near the arrowheads are π^- to π^+ ratios of the classical Jacobians (phase space factors) calculated exactly from trajectory mapping. The italic numbers midway on the solid arrow are the corresponding ratios for the approximation $J=1-\nabla\cdot\delta\vec{v}$. It is not correct to equate these ratios with common initial velocity to π^-/π^+ Coulomb ratios, since the velocity shifts are so large. One would need to divide Jacobians at the same *final* velocity.

V. THE SOURCE FUNCTION

In this section we address the fundamental but more complex problem of the initial momentum distribution of pions. Most previous studies of Coulomb effects have simply taken a Boltzmann distribution about the center of mass. Even for the high energy region of the pion spectra where

Coulomb effects are small there is a systematic excess of pions near 0° and 180° relative to 90°. Such anisotropy calls for source function refinements beyond the one-fireball model. We shall take anisotropy into account, at least qualitatively, through a two-fireball source of thermal pions. We also introduce a nonthermalized (nascent) pion source term, which should be anisotropic like $P(P,\pi^+)X$ data. However, the nascent pion contribution to the low energy pion region is small, aside from its effect in renormalizing the thermal term, and the nascent pion term was left isotropic.

The source function and geometrical factor must be used as weighting functions in summing the Monte Carlo trajectories to give pion inclusive cross sections. The source function S is proportional to the double differential cross section for π^0 production (no absorption) at a given impact parameter b.

The final c.m. pion inclusive spectra are calculated by summing over the impact parameter and weighting each impact parameter and summing over all initial pion distributions to give

$$\frac{1}{P_{\perp f}}\frac{d^2\sigma}{dP_{\perp f}dP_{\|f}}(\text{inclusive})=\int_0^{b_0}2\pi b\sum_{\vec{\beta}_\pi^{(i)},\theta_\pi}S(\beta_{\text{c.m.}},R_P^0,R_T^0,b,\vec{\beta}_\pi^{(i)})\left|\frac{\partial^3(\vec{\mathrm{P}}_i)}{\partial^3(\vec{\mathrm{P}}_f)}\right|db\ , \tag{25}$$

where $\vec{\mathrm{P}}_\nu=m_\pi\vec{\beta}_\pi^{(\nu)}/c$ $(\nu=i,f)$ is the pion momentum (nonrelativistically). From now on β is the velocity in units of c and $m_\pi c^2$ is the pion rest mass in MeV. We note again that S is a function of the beam energy (through $\beta_{\text{c.m.}}$), reaction geometry (through R_P^0 and R_T^0), impact parameter b, and pion initial velocity components $\beta_{\perp\pi}^{(i)}$ and $\beta_{\|\pi}^{(i)}$. The generalized phase space factor

$$\left|\frac{\partial^3(\vec{\mathrm{P}}_i)}{\partial^3(\vec{\mathrm{P}}_f)}\right|$$

is a kind of delta function with five arguments and it maps from the initial two momentum components of $\vec{\mathrm{P}}_i$ and the ring angle position θ_π to the final two momentum components, $P_{\|f}$ and $P_{\perp f}$. The phase space factor here will be zero for initial conditions that lead to pion absorption or orbiting. A corresponding quantum mechanical Green's function would be smeared over final momenta. By letting $b_\alpha=b=\alpha b_0$ the upper limit of integration becomes 1. We ran trajectories for $\alpha=0.1$–0.9 in steps of 0.1 as well as $\alpha=0.05$ and 0.95. One can approximate the integration from $\alpha=0.1$ to 0.9 by a summation using Simpson's rule. The region from $\alpha=0$ to 0.1 can be approximated by a triangle and trapezoidal (likewise for the region where $\alpha=0.9$ to 1.0). This is based on the fact that the product bS must be zero at $b=0$ and $b=b_0$. From the above approximation the inclusive pion distribution [right-hand side of Eq. (26)] is given by

$$(\pi b_0{}^2/15)\sum_\alpha C_\alpha\sum_{\vec{\beta}_\pi^{(i)},\theta_\pi}S(\beta_{\text{c.m.}},R_P^0,R_T^0,b,\vec{\beta}_\pi^{(i)})\left|\frac{\partial^3(\vec{\mathrm{P}}_i)}{\partial^3(\vec{\mathrm{P}}_f)}\right|\ , \tag{26}$$

where the coefficients C_α for all possible values of α are given in Table II.

Further, the source function S for a given impact parameter can be factored

$$S(\beta_{\text{c.m.}},R_P^0,R_T^0,b,\vec{\beta}_\pi^{(i)})=Y_\pi(\beta_{\text{c.m.}},R_P^0,R_T^0,b)F[\vec{\beta}_\pi^{(i)},\beta^*(\beta_{\text{c.m.}},b),T(\beta_{\text{c.m.}},b)]\ , \tag{27}$$

where Y_π is the dimensionless integrated pion yield function, namely, the average number of pions of a particular charge produced in a collision of impact parameter b. F is the initial pion-velocity distribution function per unit volume in momentum space, normalized to unity over all momentum space. The function F depends on (i) the pion initial velocity $\vec{\beta}_\pi^{(i)}$; (ii) the final speed of the fireball(s) β^*, which depends on the impact parameter b and the center of mass speed, $\beta_{\text{c.m.}}$; and (iii) the fireball(s) temperature, which in general depends on $\beta_{\text{c.m.}}$ and b.

TABLE II. Values of the modified Simpson's rule coefficients for impact parameter weighting.

α	0.05	0.1	0.2	0.3	0.4	0.5	0.6	0.7	0.8	0.9	0.95
C_α	0.075	0.175	0.8	0.6	1.6	1	2.4	1.4	3.2	1.575	1.425

A. The pion yield function Y (row-on-row model)

We shall develop a model based on concepts of Hufner and Knoll's[20] row-on-row model and Sternheim and Silbar's[21] nucleon-nucleus pion production model.

In the region of 0.4–0.9 GeV (laboratory), nucleon-nucleon elastic scattering is rather forward peaked. This forward peaking means that the rate

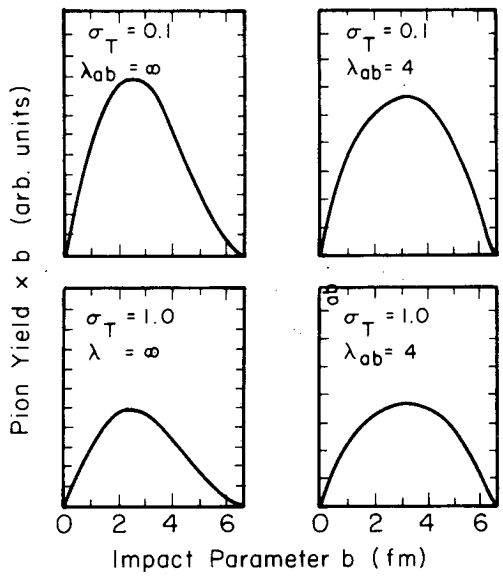

FIG. 9. Pion yield function vs impact parameter by row-on-row model with four different assumptions for parameters (^{20}Ne on ^{20}Ne). The value σ_T is related to the mean free path λ_{pr} ($=1/\rho\sigma_T$) of a nucleon in nuclear matter for the probability of producing a pion to drop to $1/e$ of its value. Parameter λ_{ab} is the mean free path for a pion to survive passage through nuclear matter without absorption.

of loss of forward momentum is slow, and one-dimensional row-on-row treatment may be justified. We simplify the row-on-row formulation by dropping all interest in momentum distributions. That is, we may integrate out the momentum distribution to determine just the probability of Δ formation.

In this energy region if the nucleon undergoes an inelastic collision to produce a Δ or pion, its kinetic energy will fall below the threshold to make a second inelastic collision. A second contribution to the decreasing probability of pion production as a nucleon penetrates a row comes as follows: Owing to forward peaking each elastic collision gives a mean energy loss of only about $\langle \Delta E \rangle^{el}=40$ MeV. Hence, there is a steady "frictional" energy loss rate in the laboratory frame due to elastic collisions

$$-\frac{dE_{lab}}{dx}=\rho\sigma_{NN}^{el}\langle \Delta E \rangle^{el} . \tag{28}$$

Also, in the energy region considered, the pion production cross section is rising with a logarithmic derivative[22]

$$\frac{d\sigma_{NN}^{in}}{dE_{lab}}\Big/\sigma_{NN}^{in}\simeq 3.805\times 10^{-3}\ (\mathrm{MeV})^{-1} .$$

Thus

$$\frac{1}{\lambda_{pr}}=\rho\left\{\sigma_{NN}^{el}\langle \Delta E \rangle^{el}\frac{d[\ln\sigma_{NN}^{in}]}{dE_{lab}}+\sigma_{NN}^{in}\right\} , \tag{29}$$

where the subscript pr on the mean free path stands for production (of pions). The pion yield function Y_π is formulated in Appendix B, and its dependence on the impact parameter is shown in Fig. 9 for the ^{20}Ne on ^{20}Ne case with $\lambda_{ab}=\infty$ and $\lambda_{ab}=4$ fm (Ref. 23) for two different values of λ_{pr}.

We note that the relative weighting of central and peripheral collisions for pion production varies with different choices of parameters. In particular, the row-on-row model with mean free paths greater than nuclear dimensions emphasize central collisions more heavily than the simple model of proportionality to a number of participant nucleons (this could be shown by comparing Fig. 9 and Fig. 2).

B. The thermal part of the pion-velocity distribution source function (the two-fireball model)

Now we should like to weight the Monte Carlo results with a more realistic model than the flat momentum distributions employed before in this paper. In the bombarding energy region considered the free nucleon-nucleon total cross section is just past its minimum, and elastic scattering is rather forward-backward peaked. Thus, the longitudinal momentum decay length λ_{lmd} of Sobel *et al.*[24] is comparable to the radius of ^{20}Ne. Their Fig. 1 shows λ_{lmd} nearly constant around 2.6 fm from 200–700 MeV. Hence, the simple one-fireball model, with its hot thermal pion source at the center of mass of the system, is not realistic. More realistic for these energies for light nuclei is the two-fireball model of Das Gupta[14] and Das Gupta and Lam.[15]

We follow the same phenomenological approach as Ref. 14 except that we use the longitudinal momentum decay length λ_{lmd} of Fig. 1 of Sobel *et al.*[24] and alternatively a value of twice this. At relativistic energies $E/A=2.1$ GeV, Heckman *et al.*[25] and El-Bakry[26] found that it was necessary to lower the effective σ_{NN} by a factor of 0.5 to get agreement in the soft spheres model with the measured interaction length of ^{16}O and ^{12}C ions in emulsion. Furthermore, Negele and Yazaki[27] have pointed out that the mean free paths of the nucleons of 50–150 MeV are experimentally about 5 fm, compared to the theory calculations, including Pauli blocking of about 3 fm. Negele and Yazaki[27] go on to resolve the discrepancy by taking proper account of the nonlocality of the nuclear optical potential.

Let us now formulate the two-fireball model in terms of Eq. (2.1) of Sobel *et al.*,[24] by a somewhat different method than that of Das Gupta.[14] Equa-

tion (2.1) of Ref. 24 could be rewritten as

$$\frac{d[\ln P_{\text{c.m.}}]}{dx} = -1/\lambda_{lmd} \ . \tag{30}$$

For nucleons in a slab of average thickness $\langle x \rangle$ we integrate to get

$$\begin{aligned} P^{(f)}_{\text{c.m.}} &= P^{(i)}_{\text{c.m.}} \exp(-\langle x \rangle / \lambda_{lmd}) \cdots \\ &= r P^{(i)}_{\text{c.m.}} \ , \end{aligned} \tag{31}$$

where $P^{(i)}_{\text{c.m.}}$ stands for incident momentum in the c.m. system and r is simply the ratio of the final c.m. momentum to the initial one. Of course, the ratio r depends on the slab thickness $\langle x \rangle$ and the longitudinal momentum decay length, λ_{lmd}, which in turn depends on the energy $\lambda_{lmd}(P_{\text{c.m.}})$.

The integration of Eq. (30) assumes λ_{lmd} is independent of the energy, which is valid according to Fig. 1 of Ref. 24 approximately between $200 \lesssim E/A \lesssim 700$ MeV in the laboratory system. Equation (31) can be applied for a slab of a number of nucleons by simply multiplying by the number of nucleons.

Let us now simplify the problem by considering only symmetric nuclei of radius R as shown in Fig. 10(a). We have previously calculated the number of participant nucleons from the projectile and target ($N = N_P + N_T$). In a symmetric system $N_P = N_T = N/2$, where N is the total number of participant nucleons for a given impact parameter b. The nonrelativistic temperature for an ideal gas of nucleons is then given by

$$T = \frac{2}{3} \frac{\Delta E_{\text{c.m.}}}{N} \ . \tag{32}$$

One can use the approximate change in the total relativistic energy, $\Delta E_{\text{c.m.}}$, of the two fireballs derived in Appendix C to get

$$\begin{aligned} T = \tfrac{2}{3} m_N c^2 \{ &[1 + \epsilon_k/(2m_N c^2)]^{1/2} \\ &- [1 + r^2 \epsilon_k/(2m_N c^2)]^{1/2} \} \ . \end{aligned} \tag{33}$$

The final velocity of the projectile and target fireballs is given by

$$\beta^* = [1 + 2m_N c^2/(r^2 \epsilon_k)]^{-1/2} \ . \tag{34}$$

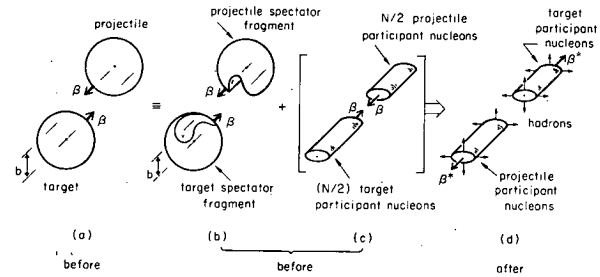

FIG. 10. Sketches illustrating the geometrical approximation used on participant pieces to get an equivalent thickness for a two-fireball model calculation. Only symmetric nuclei of radius R are considered. Fireballs are approximated as elliptical cylinders with major and minor axes matching the true cuts and with volumes equaling those of the true cuts (as described in Appendix C).

One can see that if $r = 1$, i.e., there is no longitudinal momentum loss, the final velocities are equal to the initial ones. Of course, this gives $T = 0$, which is expected for complete fireball transparency.

Figure 11 plots the numerical values calculated for β^* and temperatures T of the final two fireballs as a function of impact parameter. The $^{20}\text{Ne} + {}^{20}\text{Ne}$ system at 655 MeV/N laboratory energy is treated, and the two cases are the λ_{lmd} of Sobel *et al.*[24] and for twice that value. For comparison we show the Das Gupta and Lam[15] temperatures for the neon system, though they are not strictly comparable since they were computed for the somewhat higher laboratory energy of 800 MeV/N. Our temperatures are simple kinetic temperatures, which would be lowered if energy used in pion production was taken into account. Since we are near the threshold region for pion production, we assume this pion cooling to be small. We do not want to assume chemical equilibrium between pions and nucleons, so we cannot invoke such formulas for temperature calculations. On the other hand, the neglect of condensation into alpha particles and other composites works in the opposite direction; allowing composites raises the temperature.

After finding β^* and T from the relativistic equations we proceed to write the initial pion velocity dependence function defined in the source function S (using nonrelativistic variables) as

$$f_{\text{th}}(\beta^{(i)}, \beta^*, T) = N_{\text{th}} \left\{ \exp\left\{ -\frac{m_\pi c^2}{2T} [(\beta^{(i)}_{\|\pi} - \beta^*)^2 + \beta^{(i)2}_{\perp\pi}] \right\} + \exp\left\{ -\frac{m_\pi c^2}{2T} [(\beta_{\|\pi}{}^2 + \beta^*)^2 + \beta^{(i)2}_{\perp\pi}] \right\} \right\} , \tag{35}$$

where the normalization constant N_{th} is given by

$$N_{\text{th}} = (2\pi m_\pi T)^{-3/2}/2 \ ,$$

which has the dimensions of inverse momentum cubed.

We believe the use of the nonrelativistic

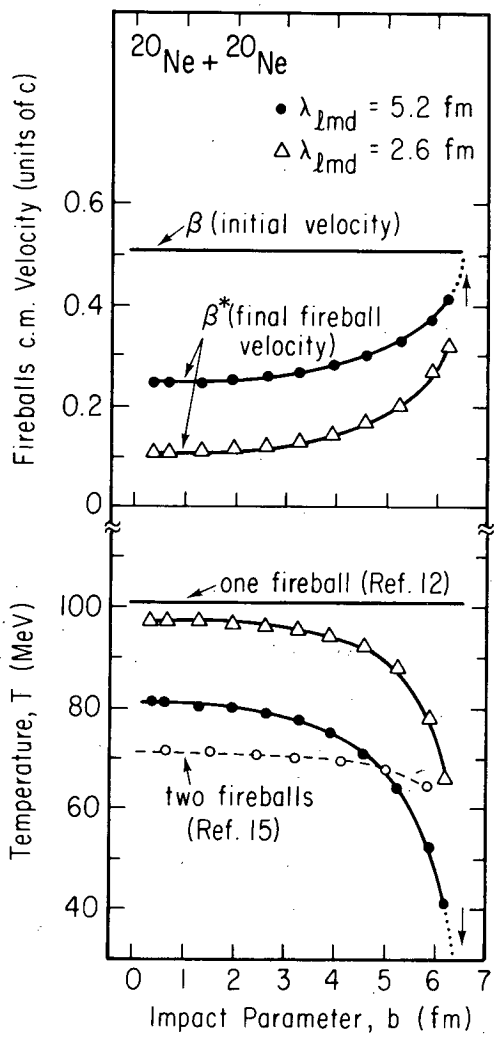

FIG. 11. Graphs showing the results of two-fireball model calculations. Open triangles use the longitudinal momentum decay length of Sobel *et al.* (Ref. 24) and solid dots use λ_{lmd} of twice this value (see text). The upper part of the figure gives the fireball velocity (c.m.) vs impact parameter, and the lower part gives the fireball temperature, with a comparison to values of Ref. 12 (straight line) and Ref. 15 (dashed line).

Boltzmann distribution is justified in our application, since we are concerned only with pions of less than 15 MeV kinetic energy in the c.m. frame.

In Fig. 12 the source function along 0° and its components are plotted for various impact parameters. As the impact parameter increases, the centers of the two fireballs move apart and the asymptotic falloff becomes greater by virtue of the lower temperature. The lower temperature raises the normalization coefficient.

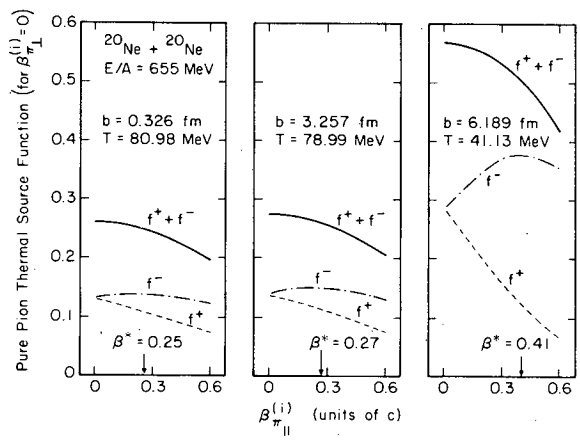

FIG. 12. Graphs illustrating the pure thermal pion source function along 0° for the two-fireball model. The signs + and − refer not to pion charge but to the contributions of projectilelike and targetlike fireballs, respectively

$$(f^{\pm}=N_{\rm th}\exp[-(\beta^{(i)}_{\parallel\pi}\pm\beta^{*})^2])\ .$$

The functions are shown for three different impact parameters.

C. Contributions of nonthermalized pions to the source function

It is a matter of some disagreement the extent to which the ratio of pions to nucleons in the fireball approaches chemical equilibrium, as assumed in certain fireball model codes. We have chosen to assume in the small ^{20}Ne+^{20}Ne system that the numbers of pions are given by the geometry of the row-on-row model, which depends on numbers of inelastic collisions and path lengths to escape from nuclear matter. This approach, in the spirit of the Sternheim-Silbar[21] p-nucleus calculations, seems favored by the observation by Nakai *et al.*[28] of prominent π^+ spectral features closely resembling $P+P=\pi^++X$. If, however, we were to base our yield function on a Boltzmann factor with the two-fireball temperature, it would likely have little effect on the overall results or conclusions of this paper. The extent to which pions and nucleons thermally equilibrate is less clearcut *a priori,* since the pion-nucleon scattering cross sections become very large near the (3,3) resonance. The data of Nakai *et al.*[28] for ^{20}Ne or NaF at E/A of 800 MeV clearly show a nonthermal (nascent) pion component, resembling $p(p,\pi^+)$ data at 730 MeV. The data of Wolf *et al.*[29] for ^{40}Ar+Ca at E/A of 1.05 GeV show the nascent pion peaks to be essentially washed out.

The above data are suggestive that the more massive system provides sufficiently longer path lengths for pions to scatter in hot nuclear matter and approach the thermal distribution.

We shall use a simple model taking a linear combination of thermal and nascent pion distributions. The proportions of these components will surely depend on the impact parameter, via a size parameter for the participant blobs. We shall take as the size parameter the cylinder thickness $\langle x(b)\rangle$ we calculated for the two-fireball formulation. The thermalization path is characterized by a λ_s for pion nucleon scattering $[\lambda_S \simeq (\rho\sigma_{NN})^{-1}]$, which we take as about 2 fm.

Thus, the source factor of Eq. (27) becomes

$$F = f_n \exp(-\langle x(b)\rangle/\lambda_S) + f_{\text{th}}[1-\exp(-\langle x(b)\rangle/\lambda_S)] \tag{36}$$

with f_{th} given by the two-fireball model expression Eq. (35) and the nonthermalized f_n taken as an expansion of a pure p-wave simplified isobar model.[30]

We made some numerical studies of the normalization integral with the Δ-resonance denominator. We found for $\beta = 0.5$ or less the pion spectrum normalization is well approximated by assuming the nascent pion spectrum is purely $P_\pi{}^2$ up to sharp cutoff at $P_{\max}$.

$$1/N_n \approx \int_0^{P_{\max}} P_\pi{}^2 P_\pi{}^2 dp_\pi = P_{\max}{}^5/5 \ .$$

This approximation is valid for the low bombarding energies where the resonance lies near or beyond $P_{\max}$, the maximum momentum (c.m.) that a pion can have from a nucleon-nucleon collision at a given energy. We have not folded in Fermi motion for the nascent pion spectrum, since such folding would not strongly affect the normalization or low-energy portion of the spectrum.

Figure 13 shows 0° cuts of the two-fireball thermal-plus-nascent pion source function for three impact parameters. The nascent pion contributions are small relative to the thermal pions for the low pion energies we treat. However, the nascent pion spectrum puts most of the pions out at large momenta and thus significantly lowers the normalization of the thermal pions as one goes to a large impact parameter. This effect can be clearly seen by comparing Figs. 12 and 13.

VI. FINAL RESULTS AND COMPARISON WITH DATA

In order to compare with pion inclusive data of ^{20}Ne on NaF at E/A of 655 MeV, the detailed two-fireball source function described above was used to construct the weighting function for the $\simeq$100 000

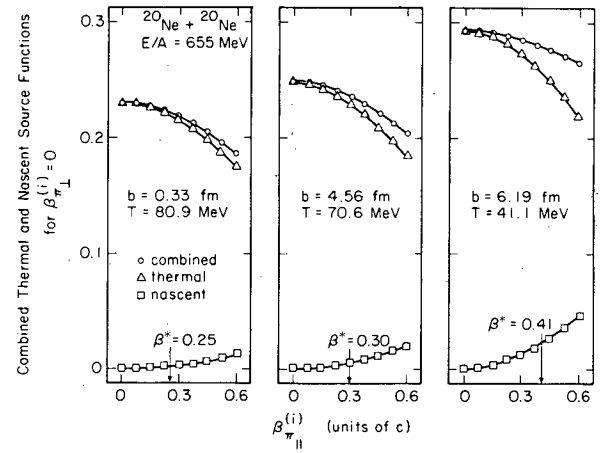

FIG. 13. Graphs illustrating the 0° contributions of thermalized and nonthermalized (nascent) pions. The separate contributions and the total are shown for the three impact parameters. This source function is that used to weight Monte Carlo results.

Coulomb surviving trajectories for each type of pion and for each impact parameter. Thus, they were combined with appropriate weighting for the various impact parameters to yield results to compare with pion inclusive data.

In Fig. 14 are plotted the surviving percentages of trajectories (for about 12 000 trials for each type of pion and for a given impact parameter) as a function

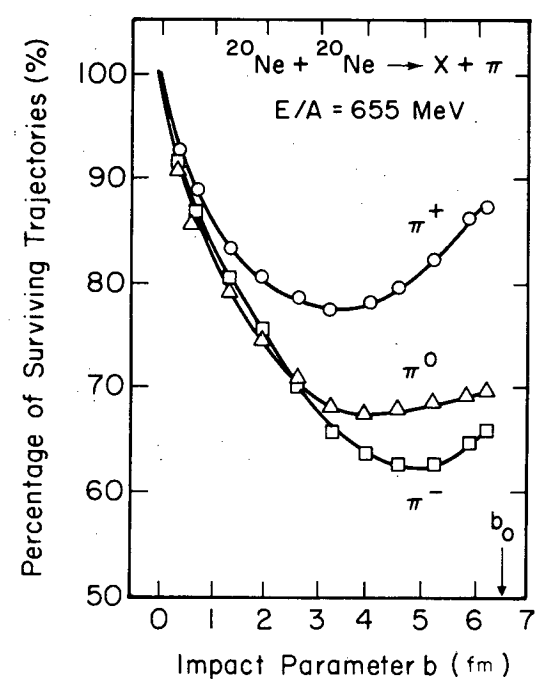

FIG. 14. Plot of the surviving percentage of Monte Carlo trajectories for the three different pion charges as a function of the impact parameter.

of impact parameter. As discussed earlier in connection with the scatter plots of Fig. 6, trajectories of all three charge states are lost to "absorption" if they pass within $0.8R$ of a spectator center, the factor 0.8 being chosen rather arbitrarily as inside the surface region. Furthermore, additional π^- trajectories are lost to orbiting. In our model there is no loss at zero impact parameter, since the spectator nuclei have become vanishingly small, and hot participant matter is neglected. The final weighted averages of the Monte Carlo trajectories are displayed in the next several figures.

In Fig. 15 spectra of π^0 vs $\beta_\perp$ are plotted for five fixed ranges of $\beta_{||}$; that is, the spectra are vertical cuts on a $\beta_\perp$ vs $\beta_{||}$ plane. Each bin is divided by its volume in three-dimensional velocity space to give differential cross sections $E_\pi d^3\sigma/dP^3$, normalized to agree with π^- data, as discussed shortly. Lorentz-invariant cross sections $E_\pi d^3\sigma/dP^3$ will be essentially the same in this low energy region, where the relativistic total energy E_π is approximately constant ($m_\pi c^2$). The π^0 cross sections are flat. The statistical uncertainty of low $\beta_\perp$ points is the greatest, since by geometrical weight the fewest events are in these bins (see Fig. 6). The width of the slices in $\beta_{||}$ is 0.1, and is only slightly larger than the quoted experimental resolution of Sullivan *et al.*[31] The last interval $\beta_{||}=0.46$–0.56 is chosen to center about the beam velocity.

Figure 16 shows the corresponding $\beta_\perp$ spectra for π^-. The peak at beam velocity in the lowest curve is as expected. The data[8] at $90°\pm5°$ in the c.m. are plotted for comparison with the first spectrum. Of course, the positions of momentum space included

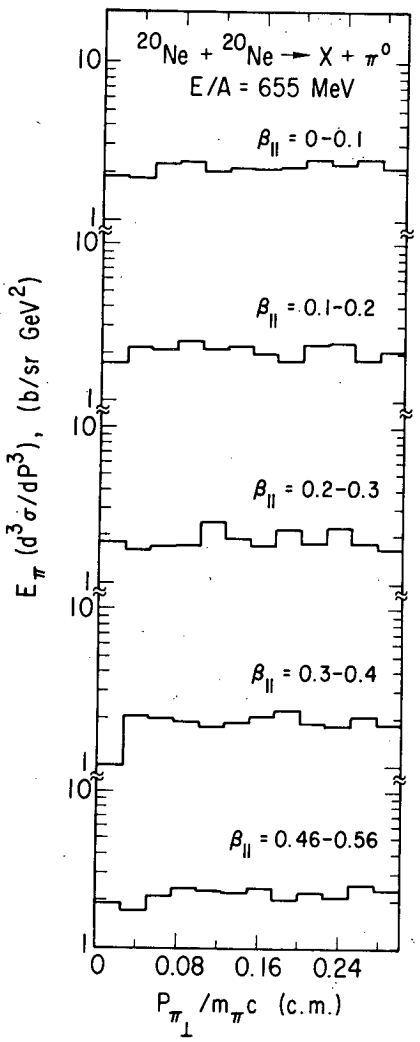

FIG. 15. Histograms of the final Monte Carlo π^0 vs $\beta_\perp$ for five different cuts of width 0.1c. Uppermost is at c.m. and lowermost is centered about the beam velocity. The normalization is the same as the one used in Fig. 16.

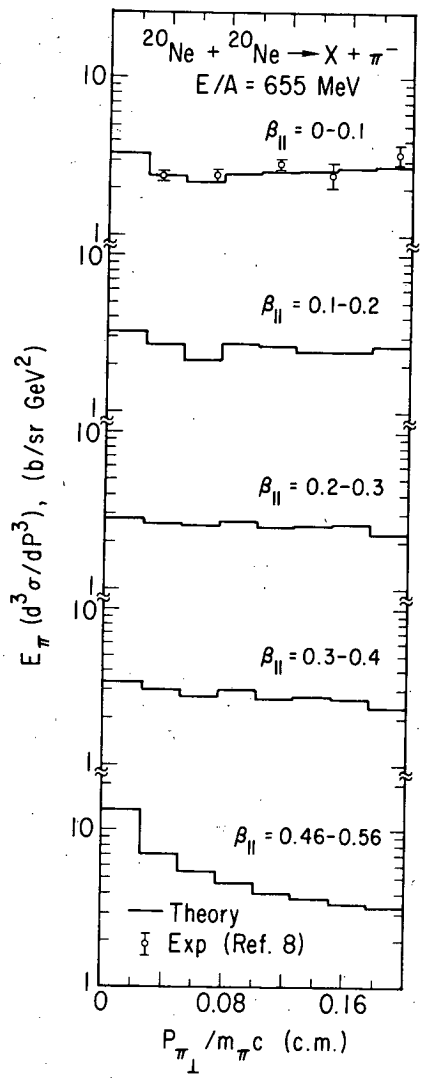

FIG. 16. Same as Fig. 15 except for π^-. The data for 90° c.m. ^{20}Ne+NaF are shown in the top graph with theory normalized to these data.

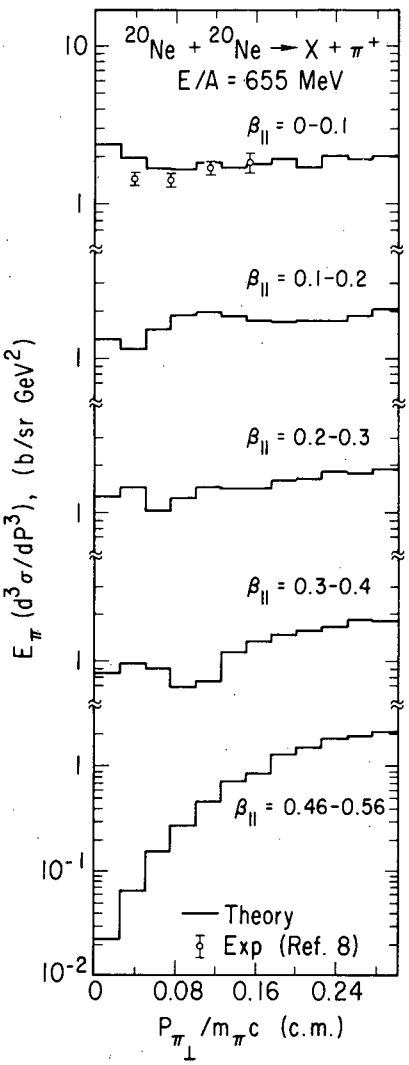

FIG. 17. Same as Fig. 16 except for π^+. The same normalization as for Fig. 16 was used.

by data and theory are not quite the same but are comparable when experimental resolution is taken into account. Furthermore, the velocity-space matching and resolution are not important for flat spectra. The small peak at c.m. (the lowest bin of the top spectrum), if real, would have been washed out by experimental resolution and perhaps also the lack of symmetry in the Ne+NaF experiment.

For the π^+ spectra in Fig. 17 there is the expected deep depression at beam velocity (the lowest curve). Indeed, the beam velocity spectrum at the bottom of Fig. 17 has a compressed scale in order to display the curve.

One normalization constant for Figs. 15–17 was fixed to match the π^- data. The π^+ theoretical curve is slightly high for the lowest two bins of the top spectrum of Fig. 17 as compared with experiment.[8] However, it should be noted that the comparison with data on these plots is mainly to be taken for slope comparisons. The theoretical ratio of π^- to π^+ still needs to be corrected for the 10% neutron excess in NaF compared to the theoretical ^{20}Ne target. Also, correction for the participant ("hot") charge still needs to be made. Later in this paper we estimate corrections for the neutron excess in NaF and for the hitherto-neglected effect of participant charge.

As mentioned above, we chose the velocity range in our plots comparable to the energy and angular resolution of Sullivan *et al.*[31] Thus, we can directly compare to the experimental Lorentz-invariant differential cross sections $E_\pi d^3\sigma/dP^3$, which we shall also do here for the 0° spectra, and we plot against β. The relativistic total energy E_π varies by less than 25% over the pion energy range considered.

Figure 18 compares experiment and theory for π^- at 0°, with the theory being multiplied by an arbitrary factor (different than the one used for the previous three figures) to give matching in the flat region. There is a reasonable agreement with the beam velocity peak in position and width, but the theoretical peak rises somewhat higher above the base than the experimental. Somewhat surprising is a secondary bump near "$\beta_{\parallel}$" of 0.13, evident in both experiment and theory.

Figure 19 compares experiment and theory for π^+ at 0°. The scale is correct for the data, and the

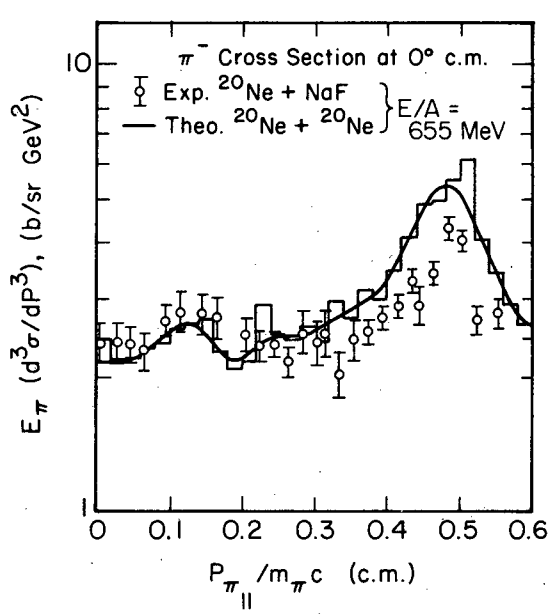

FIG. 18. Cut along 0° for π^-. The theory is shown both by a histogram and a computer-smoothed curve. The width of the cut is β to 0.1c, comparable to experimental resolution. Data are plotted with error bars and the theory has been normalized to the flat portion.

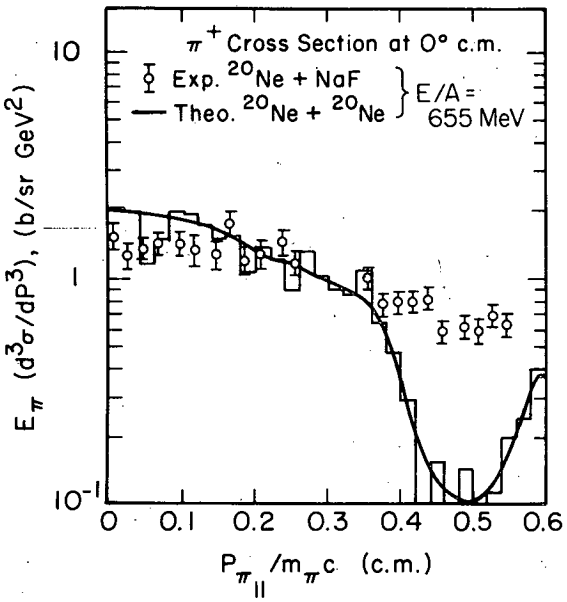

FIG. 19. Same as Fig. 18 except for π^+. The normalization constant for the theory is the same as for Fig. 18.

normalization factor applied to the theory is the same as that in Fig. 18 for the π^-. Thus, π^-/π^+ ratios may be graphically estimated. The π^+ data at c.m. are somewhat below theory, but as discussed for Fig. 17 the subsequent corrections for neutron excess and for participants raise the π^+ points to agreement at c.m.

For the π^+ the theoretical curve is not as flat as the experimental, and the beam velocity minimum is too low in the theory. We have varied the impact-parameter weighting and can get slightly better agreement for unrealistically strong weighting of central collisions. The more likely explanation of the discrepancy is the neglect of quantum effects. The region of the π^+ beam velocity minimum will be most sensitive to the neglect of quantum mechanical effects, for these slow-moving pions in the projectile frame spend appreciable time near the projectile and have wavelengths in this frame long compared to nuclear dimensions.

A. The π^-/π^+ ratio at center of mass

Finally, we critically examine the main question that prompted this theoretical study, namely, what π^-/π^+ ratios are predicted at and near center-of-mass velocity. Since the theoretical π^+ and π^- spectra are not flat near the center of mass and the statistics are limited, care must be taken in choosing the momentum intervals over which to average. We have chosen to average in such a way as to compare with data of Sullivan.[8] The experimental ratios show some fluctuation from point to point around the center of mass, but there is no systematic trend. Thus, we average the π^-/π^+ ratio for 18 data points surrounding the center of mass, namely, six momenta (laboratory) from 74 to 96 MeV/c and 0°, 4°, and 8° (laboratory). The average of these ratios is 1.76 ± 0.1. These momentum and angular ranges correspond approximately to limits of $\beta_{\parallel}$ and $\beta_{\perp}$ from 0 to 0.1.

We determine the theoretical spectator effect ratio first by averaging the π^-/π^+ ratios of nine bins about the same size as experimental bins. This average of ratios is 1.40.

In comparing theoretical and experimental π^-/π^+ ratios it is necessary to take into account that the experimental systems studied have a neutron excess. Quite aside from Coulomb effects, the neutron excess will produce an excess of π^- over π^+ in what we will call the "primitive" π^-/π^+ ratio. The primitive ratio is also model dependent. We shall assume the (3,3) isobar and row-on-row models. We shall assume the ratio is not altered by charge exchange scattering, consistent with our earlier assumption of thermal but not chemical equilibrium between pions and nucleons. Sternheim and Silbar[21] did need to include charge exchange scattering for π^- from proton-nucleus reactions, but their ratio of pions formed initially is very deficient in π^- because the projectile has maximal isobaric asymmetry (no neutrons).

Sullivan,[8] following Sternheim and Silbar,[21] using Clebsch-Gordan branching relations for Δ decay, has given Eqs. (6.8) and (6.10) from which we get the primitive π^-/π^+ ratio.

$$Y_-/Y_+=(10N_PN_T+Z_TN_P+N_TZ_P)/(10Z_PZ_T+Z_TN_P+N_TZ_P)\ .$$

For ^{20}Ne+^{21}Ne (average target nucleus) we get

$$Y_-/Y_+=131/121=1.083\ .$$

We need to assess the effects of participant charge on the ratio. It is not straightforward to calculate this effect, since the pions and protons do not start from a common center. However, we shall make an estimate by the following model: Let the fireball protons begin expanding with speed v_c in a uniformly charged spherical shell at some mean radius R_c ($0.6r_0A^{1/3}$). Let the pion start from the surface R_r ($r_0A^{1/3}$ with $r_0=1.2$ fm). In order to have a final velocity of zero a π^- must have a radial outward speed of v_i. The pion will experience at first

an attractive Coulomb force, but the force suddenly goes to zero as the proton shell passes the pion. We can, by simple algebra, derive the dependence of the final π^- velocity v_{xf} on the initial velocity v_{xi}.

$$v_{xf}=v_c-[(v_c-v_i)^2+2a(R_r-R_c)]^{1/2}\ , \tag{37}$$

where a is the magnitude of the acceleration, here considered constant since the pion has low velocity, and the force from the shell acts from the origin.

$$a=Ze^2/mR_r^{\,2}\ .$$

The Jacobian (or Coulomb phase space factor) becomes

$$J_-=\begin{vmatrix} \dfrac{\partial v_{xf}}{\partial v_{xi}} & 0 & 0 \\ 0 & 1 & 0 \\ 0 & 0 & 1 \end{vmatrix}^{-1}=\left[\frac{\partial v_{xf}}{\partial v_{xi}}\right]^{-1}.$$

For the case of interest here $v_i \ll v_c$; hence, the cross derivatives in the Jacobian determinant approach zero and the diagonal elements for the perpendicular directions go to unity.

Differentiating Eq. (37) gives the result

$$J_\mp=\left[1\mp\frac{2a(R_r-R_c)}{(v_c-v_i)^2}\right]^{-1/2}$$

$$\approx 1\pm\frac{Ze^2}{R_r m(v_c-v_i)^2}\frac{(R_r-R_c)}{R_r}\ , \tag{38}$$

where we have indicated also the result for π^+ by the lower signs. For a numerical estimate we approximate the participant charge and size for an average impact parameter leaving half the total charge in the fireball. We take $Z=10$ and $R_c=1.2\times 20^{1/3}=3.26$ fm. The mean velocity of the expanding fireball we take as the original c.m. value $\beta=0.51$, ignoring pion cooling effects. From this we calculate that $v_i=0.025$ with

$$J_-=1+0.054 \text{ and } J_+=1-0.054\ . \tag{39}$$

That is, the participant (fireball) charge contributes a factor of 1.11 to the π^-/π^+ ratio at the c.m. Multiplying these factors, 1.083 for neutron excess, 1.40 for spectators, and 1.11 for participant charge, we get a theoretical π^-/π^+ c.m. ratio of 1.68.

This ratio is in quite satisfactory agreement with the ratio of 1.76 ± 0.1 calculated, as described earlier in this section, from data tabulated by Sullivan.[8]

Time and resources were not sufficient for us to run other than exploratory Monte Carlo calculations on other systems, such as ^{40}Ar+^{40}Ca and ^{238}U+^{238}U.

Consider now the experimental measurement of the central π^-/π^+ ratio in ^{40}Ar+^{40}Ca at E/A of 1.05 GeV. The ratio is essentially the same as for ^{20}Ne+NaF at E/A of 655 MeV. In lieu of detailed Monte Carlo calculations on Ar+Ca we use our Eq. (38) and the very similar formula of Ref. 4 to scale spectator Coulomb effects as

$$ZR^{-1}k^{-2}\approx A^{2/3}(\gamma_{\text{c.m.}}-1)^{-1}\ ,$$

where Z is the charge, R is the nuclear radius, and k is the wave number (momentum) of a pion moving with beam velocity in the c.m. frame. When we apply this scaling law, we find that the increased charge of the Ar+Ca experiment is more than compensated by the higher energy. These comparisons are summarized in Table III.

It is interesting to note the similarity of Eq. (38) to the classical expression (2.15) of Gyulassy and Kauffmann.[4] If we neglect v_i compared to v_c, a good approximation, our correction term to the Jacobian differs from theirs only by being reduced by the factor $(R_r-R_c)/R_r$, a factor of 2 or 3 reduction, depending on the choice of mean initial radii for protons and pions as expansion begins and nuclear charge exchange equilibrium with pions is lost. If we start proton expansion at the origin, our expression reduces to theirs for the special case of pions at the c.m.

We believe that the various Coulomb correction formulas for pions near the projectile velocity, as applied by Gyulassy and Kauffmann,[4] by Sullivan *et al.*,[31] and by Radi *et al.*[6] are justified. The projectile spectator is bound or weakly excited to evaporate a few protons, and the charge of the one spectator dominates the Coulomb correction on pions near it in velocity space.

On the other hand, we hold reservations about analytical expressions hitherto applied to pion Coulomb corrections at midrapidity, such as the regular Coulomb function applied by Siemens and Rasmussen[32] and the perturbative formulas of Gyulassy and Kauffmann,[4] based on expansion of

TABLE III. Zero energy (c.m.) π^-/π^+ ratio factors.

	^{20}Ne+NaF at 655A MeV	^{40}Ar+Ca at 1050A MeV
Spectator Coulomb factor	1.40	1.36[a]
Neutron-excess factor	1.083	1.17
Participant Coulomb factor	1.11	1.10
Final product	1.68	1.75
Experiment (Ref. 7)	1.76±0.1	1.5±0.2

[a]Calculated by scaling from ^{20}Ne Monte Carlo results.

charged particles from a common origin.

We have a disagreement for very slow pions (c.m.) with Gyulassy-Kauffmann expressions for the grazing impact parameter, where the pion starts exactly midway between the spectator charge centers. In this case, we found Jacobians very close to unity for π^- and π^+. However, our final result for the central π^-/π^+ ratio of 1.68 is fortuitously close numerically to the result of using their expressions. Apparently the location of pion starting points off the line of centers spoils the cancellation of Coulomb effects. There is certainly a complicated vector addition of Coulomb forces that makes it doubtful that the effects can be expressible as a sum of scalar terms for the various moving charge centers.

Certainly much work remains to be done to understand the Coulomb effects on heavy-ion pion spectra. Future Monte Carlo studies ought to be relativistic and extend to higher pion momenta to connect with the wealth of data from Nagamiya *et al.*[33]

One should treat spectator and participant charge on the same footing. In this regard it would be desirable to have a rerun of the Cugnon and Koonin[3] Monte Carlo calculations with the pion source function modified and absorption within a certain density of nuclear matter taken into account. That is, it would be desirable to have the spatial part of the source function concentrated on the surface of the interactive volume, namely outside the nuclear density, at which pion-nucleon charge exchange reactions are prevalent. We are not able to compare directly with their results, since our calculation is for the ^{20}Ne+^{20}Ne system at $E/A=655$ MeV and theirs is for a system of double the charge and at higher energy. We can only speculate that their peak in the π^-/π^+ ratio at c.m., which is contrary to subsequent experiment, perhaps arises from pions formed near the origin with small velocities. Their central fireball potential will provide an attractive well for π^- and a repulsive hill for π^+. It could also be that quantum effects could be significant in suppressing sharp peaks or valleys in the distributions.

Going yet a step beyond the Cugnon and Koonin[3] Monte Carlo work, one might run a nucleus-nucleus cascade code and for each event carry out the Coulomb modified trajectories of the pions. Of course, it would be desirable to have such calculations for more than one energy or Z value. Although we did not have time to run the calculation for many variations in source function parameters, it is likely that the final results are not very sensitive to the several parameters in our source function. We did wish to formulate a fairly complete source function, although it remains for further work to match high-energy pion spectra not treated here.

One may be suspicious of classical calculations of low energy pions, since wavelengths exceed nuclear dimensions. However, in recent years much has been done to bring in quantal effects through the classical action integral. We are doubtful that quantal interference effects would survive averaging over the large number of final states. As we pointed out, though, the neglect of quantal effects probably led us to exaggerate the beam velocity π^+ depression, a problem that needs attention in future work.

ACKNOWLEDGMENTS

We thank M. Gyulassy, W. Zajc, and Jakob Bondorf for useful suggestions and discussions. One of the authors (H.R.) would like to thank the Physics Department of Kuwait University for granting him a leave to be spent at Lawrence Berkeley Laboratory (LBL). We are appreciative of the LBL management decision that temporarily made substantial computer time available without recharge and thus made possible the work of this paper. This work was supported by the Director, Office of Energy Research, Division of Nuclear Physics of the Office of High Energy and Nuclear Physics of the U. S. Department of Energy under Contract DE-AC03-76SF00098.

APPENDIX A: SPECTATOR CENTROID SHIFTS AND THE RADIUS OF MAXIMUM OVERLAP RING

For simplicity, we compute the shift of center of mass of the spectators by scraping out segments of maximum height S as seen from Fig. 20. In this figure the geometry gives us the shift of the new centroids, δb, with respect to the original centers as follows:

$$b_i=\frac{S^2[18R_i^{0^2}-16R_i^0S+S^2]}{4[4R_i^{0^3}-3R_i^0S^2+S^3]} \quad (i=P,T)\ , \quad \text{(A1)}$$

where $S=R_P^0+R_T^0-b$.

The radius of the maximum overlap ring, R_r, and the distance between the center of this ring and the center of the original projectile spectator fragment, d, can be found from geometry as

$$R_r=2[S(S-R_P^0)(S-R_T^0)(S-b)]^{1/2}/b\ , \quad \text{(A2)}$$

$$d=[(R_P^0)^2-R_r{}^2]^{1/2}\ , \quad \text{(A3)}$$

where S in Eq. (A2) is given by

$$S=(R_P^0+R_T^0+b)/2\ .$$

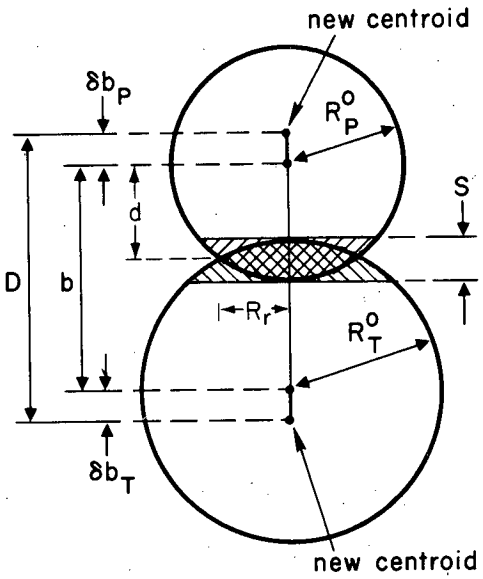

FIG. 20. Sketch illustrating the geometry of calculation of centroids of spectator fragments.

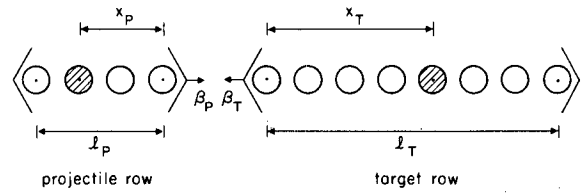

FIG. 21. Sketch of row-on-row one-dimensional geometry with parameters identified.

APPENDIX B: ROW-ON-ROW MODEL FOR PION YIELD FUNCTION

As a simplified version of the row-on-row model, let us start by assuming two interacting rows of lengths l_P and l_T (representing projectile and target, respectively). The nucleons in a row are spaced by a mean free path, λ, when one considers a row of a cross-sectional area σ_{NN}^{tot}

$$\lambda=\frac{1}{\rho\sigma_{NN}^{\text{tot}}} . \tag{B1}$$

The situation is schematically shown in Fig. 21. We assume that the probability of producing a pion by the first nucleon in the projectile row, incident on a nucleon at a distance x_T from the first nucleon in the target row, is given by an exponentially decreasing function of distance as

$$P_{\text{pr}}(x_P=0,x_T)=\sqrt{a_{\text{pr}}}e^{-x_T/\lambda_{Pr}} , \tag{B2}$$

where $x_P=0$ indicates the first nucleon in the projectile row and x_T indicates the mth, for instance, nucleon in the target row (then $m=x_T/\lambda+1$). In Eq. (B2) λ_{pr} is the pion production mean free path defined by Eq. (29) and a_{pr} is a proportionality constant. By symmetry the attenuation of cross section for trailing nucleons in the projectile row also falls exponentially. The pion production from two nucleons, one at x_P in the projectile row and the other at x_T in the target row, is now

$$P_{\text{pr}}(x_P,x_T)=a_{\text{pr}}e^{-(x_P+x_T)/\lambda_{\text{pr}}} . \tag{B3}$$

The overall probability for two rows of length l_P and l_T is simply obtained after integrating Eq. (B3) over $dx_P dx_T$ to have

$$P_{\text{pr}}(l_P,l_T)=a_{\text{pr}}\lambda_{\text{pr}}^2[1-\exp(-l_P/\lambda_{\text{pr}})] \times[1-\exp(-l_T/\lambda_{\text{pr}})] . \tag{B4}$$

The next step is to apply Eq. (B4) to a specific reaction. Let us assume a projectile of radius R_P^0 and target of radius R_T^0 (we will drop the superscript 0 in the formulas for convenience). In the center-of-mass frame they are moving with β_P and β_T, respectively. In part (a) of Fig. 22 we display the geometry of the reaction with the differential element of two disks at height y from the center of the target. In part (b) two rows in the interacting disks are shown. One can get the total pion production probability by integrating over all possible y and z variables to get

$$P_{\text{pr/tot}}(R_P,R_T,b)=2\int_{y=b-R_P}^{y=R_T}dy\int_{z=0}^{r_{PT<}}dz\,P_{\text{pr}}\{l_P=2[R_P{}^2-(b-y)^2-z^2]^{1/2},l_T=2[R_T{}^2-y^2-z^2]^{1/2}\} , \tag{B5a}$$

where

$$r_{\text{PT}_<}=\begin{cases} r_P=[R_P{}^2-(b-y)^2]^{1/2} , \text{ if } r_P<r_T , \\ r_T=[R_T{}^2-y^2]^{1/2} , \text{ if } r_T<r_P . \end{cases} \tag{B5b}$$

The integrand of the integral of Eq. (B5a) is shown on the left side of Fig. 23 for $b=0.3(R_P+R_T)$ for the ^{20}Ne on ^{20}Ne system. On the right side a projection along the y axis is shown. The pion production

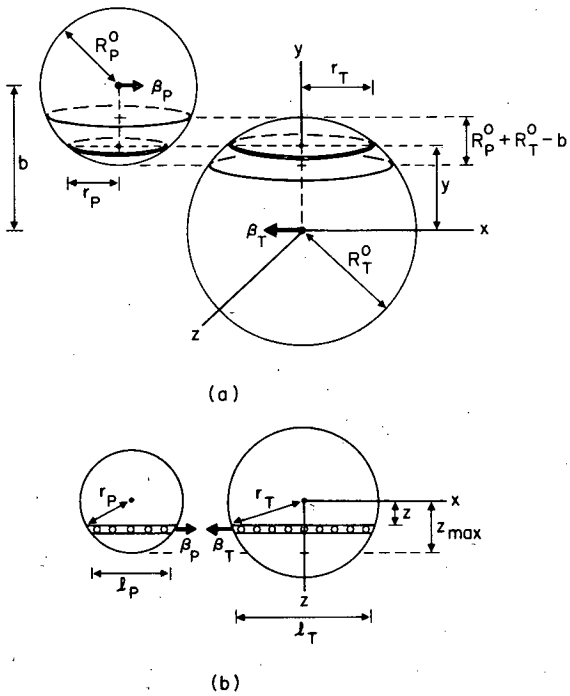

FIG. 22. Sketch of three-dimensional row-on-row geometry for calculation of pion yield at a given impact parameter (see text).

mean free path is taken to be $\lambda_{pr}=\lambda$ as given by Eq. (B1) and calculated at 655 MeV/nucleon (laboratory).

Since pions produced well into the middle of the projectile and target rows have less chance to appear on the surface, then in the spirit of the Sternheim-Silbar model,[21] one should allow pions to be absorbed also. If we consider the case given by Eq. (B3) and refer to Fig. 21, we see that a pion produced nearly at rest from a nucleon at a distance x_T in the target row and a nucleon at a distance x_P in the projectile row must survive passage of a length (l_T-x_T) of the target row and survive (l_P-x_P) of the projectile row to be observable. As seen from Fig. 1 of Hecking,[23] pion mean free paths are never negligibly long. If λ_{ab} stands for the pion absorption mean free path, then the probability of forming a pion at x_T (in the target row) from a nucleon at x_P (in the projectile row) and surviving thickness (l_T-x_T) in the target row and (l_P-x_P) in the projectile row is written as

$$P(x_P,x_T)=a_{pr}^{ab}\exp[-(x_P+x_T)/\lambda_{pr}] \times\exp[-(l_P-x_P)/\lambda_{ab}] \times\exp[-(l_T-x_T)/\lambda_{ab}] , \quad \text{(B6)}$$

where a_{pr}^{ab} is a proportionality constant. Upon integration over $dx_P dx_T$ we get

$$P_{pr}^{ab}(l_P,l_T)=a_{pr}^{ab}\lambda_{pr}^{ab^2}\exp[-(l_P+l_T)/\lambda_{ab}] \times[1-\exp(-l_P/\lambda_{pr}^{ab})] \times[1-\exp(-l_T/\lambda_{pr}^{ab})] , \quad \text{(B7a)}$$

where

$$\lambda_{pr}^{ab}=\lambda_{pr}/[1+(\lambda_{pr}/\lambda_{ab})] \underset{\lambda_{ab}\to\infty}{\longrightarrow} \lambda_{pr} . \quad \text{(B7b)}$$

As in the case of no absorption ($\lambda_{ab}=\infty$) the total observable pion production is symbolically denoted by $P_{pr/tot}^{ab}(R_P,R_T,b)$ and could be calculated by replacing Eq. (B5a) by the right hand side of Eq. (B7a). The pion yield function is generally the total pion production probability per nucleus-nucleus collision

$$Y_\pi(\beta_{c.m.},R_P,R_T,b)=P_{pr/tot}^{ab}(R_P,R_T,b) . \quad \text{(B8)}$$

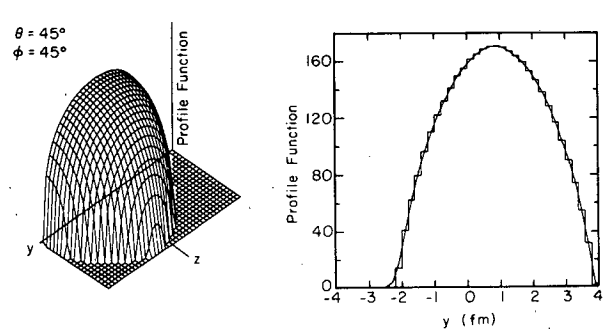

FIG. 23. Plots of the integrand in the integral for the pion yield function [Eq. (B5a)] at a given impact parameter (see text). Coordinates are defined in Fig. 22. On the right-hand side a projection onto the y axis is displayed.

APPENDIX C: GEOMETRICAL APPROXIMATION USED FOR THE TWO-FIREBALL MODEL

For a given impact parameter we let $N/2$ nucleons from the projectile or the target fill a cylindrical slab of thickness $\langle x\rangle$. This cylindrical slab, which represents the overlapping matter, will be considered as an elliptical cylinder with an area of an ellipse of semimajor and semiminor axes that are the same as for the fireball cylindrical cuts. These lengths are given [as shown in part (c) of Fig. 10] by the following:

$$\text{semimajor axis}=(R^2-b^2/4)^{1/2} , \quad \text{semiminor axis}=R-b/2 . \quad \text{(C1)}$$

To find an average slab thickness $\langle x\rangle$ we use the volume as related to the number of participant nu-

cleons, $N/2$, for each fireball. Then

$$\langle x \rangle = N/[2\pi\rho(R-b/2)(R^2-b^2/4)^{1/2}] \ . \tag{C2}$$

Hence, for the impact parameter b under consideration the ratio

$$r = \exp(-\langle x \rangle/\lambda_{lmd})$$

is given. For such a symmetric system the center-of-mass velocity with respect to laboratory is a special case of Eq. (1) and is given by

$$\beta_{\text{c.m.}} = [1+2m_N c^2/\epsilon_k]^{-1/2} \ , \tag{C3}$$

where $m_N c^2$ and ϵ_k are already defined in Sec. II. The initial velocity of the projectile and target fireballs in the center-of-mass frame are identical to $\beta_{\text{c.m.}}$ for such a symmetric system,

$$\beta^{(i)}_{\text{c.m.}}(\text{pf}) = \beta^{(i)}_{\text{c.m.}}(\text{tf}) = \beta_{\text{c.m.}} = \beta \ , \tag{C4}$$

where the notations pf and tf stand for the projectile fireball and the target fireball, respectively. The initial target fireball momentum in the center-of-mass frame is given as

$$P^{(i)}_{\text{c.m.(pf)}} = \gamma_{\text{c.m.}}[P^{(i)}_{\text{lab(pf)}} - \beta_{\text{c.m.}} E^{(i)}_{\text{lab(pf)}}] \ , \tag{C5}$$

where

$$\gamma_{\text{c.m.}} = 1/(1-\beta_{\text{c.m.}}{}^2)^{1/2} \ ,$$

and where the initial momentum and total energy of the projectile fireball in the laboratory are given by

$$P^{(i)}_{\text{lab(pf)}} = \frac{N}{2}\epsilon_k[1+2m_N c^2/\epsilon_k]^{1/2} \ , \tag{C6a}$$

$$E^{(i)}_{\text{lab(pf)}} = \frac{N}{2}\epsilon_k[1+m_N c^2/\epsilon_k] \ . \tag{C6b}$$

The above equations give

$$P^{(i)}_{\text{c.m.(pf)}} = \frac{N}{2}\epsilon_k[m_N c^2/(2\epsilon_k)]^{1/2} \ . \tag{C7}$$

Using Eq. (31), we get the final total energy of the projectile fireball in the center of mass to be

$$E^{(f)}_{\text{c.m.(pf)}} = \frac{N}{2} m_N c^2[1+r^2\epsilon_k/(2m_N c^2)]^{1/2} \ .$$

One can now find the change in the total relativistic energy of the two fireballs (the conditions of the target fireball are the same as the projectile fireball for any symmetric system) as

$$\Delta E_{\text{c.m.}} = N m_N c^2\{[1+\epsilon_k/(2m_N c^2)]^{1/2} - [1+r^2\epsilon_k/(2m_N c^2)]^{1/2}\} \ . \tag{C8}$$

The final velocity of the projectile and target fireballs is given by

$$\beta^{(f)}_{\text{c.m.(pf)}} = \beta^{(f)}_{\text{c.m.(tf)}} = [1+2m_N c^2/(r^2\epsilon_k)]^{-1/2} = \beta^* \ . \tag{C9}$$

---

*Present address: Cyclotron Institute, Texas A&M University, College Station, TX 77843.

[1]W. Benenson, G. Bertsch, G. M. Crawley, E. Kashy, J. A. Nolen, Jr., H. Bowman, J. G. Ingersoll, J. O. Rasmussen, J. Sullivan, M. Koike, M. Sasao, J. Péter, and T. E. Ward, Phys. Rev. Lett. 43, 683 (1979).

[2]K. G. Libbrecht and S. E. Koonin, Phys. Rev. Lett. 43, 1581 (1979).

[3]J. Cugnon and S. E. Koonin, Nucl. Phys. A355, 477 (1981).

[4]M. Gyulassy and S. K. Kauffmann, Nucl. Phys. A362, 503 (1981).

[5]G. Bertsch, Nature 283, 280 (1980).

[6]H. M. A. Radi, J. O. Rasmussen, J. P. Sullivan, K. A. Frankel, and O. Hashimoto, Phys. Rev. C 25, 1518 (1982); J. O. Rasmussen, H. M. A. Radi, J. P. Sullivan, K. A. Frankel, and O. Hashimoto, Proceedings of the Fifth High Energy Heavy Ion Study, Berkeley, 1981, Lawrence Berkeley Laboratory Report LBL-12652-UC-34 Conf-8105-104, p. 397.

[7]K. A. Frankel, J. A. Bistirlich, R. Bossingham, H. R. Bowman, K. M. Crowe, C. J. Martoff, D. Murphy, J. O. Rasmussen, J. P. Sullivan, W. A. Zajc, J. P. Miller, O. Hashimoto, M. Koike, J. Péter, W. Benenson, G.

M. Crawley, E. Kashy, J. A. Nolen, Jr., and J. Quebert, Phys. Rev. C 25, 1102 (1982); also Phys. Rev. C (to be published).

[8]J. P. Sullivan, Ph.D. thesis, University of California, Lawrence Berkeley Laboratory Report No. 12546, 1981 (unpublished).

[9]D. E. Greiner, P. J. Lindstrom, H. H. Heckman, Bruce Cork, and F. S. Bieser, Phys. Rev. Lett. 35, 152 (1975).

[10]A. S. Goldhaber, Phys. Lett. 53B, 306 (1974).

[11]Theoretical work has been done on such fragmentations by J. Hufner, K. Schäfer, and B. Schurmann, Phys. Rev. C 12, 1888 (1975); A. Abul-Magd, J. Hufner, and B. Schurmann, Phys. Lett. 60B, 327 (1976); A. Abul-Magd and J. Hufner, Z. Phys. A 277, 379 (1976).

[12]The early development of the fireball model for heavy ions was by G. D. Westfall, J. Gosset, P. J. Johansen, A. M. Poskanzer, and W. G. Meyer, Phys. Rev. Lett. 37, 1202 (1976); J. Gosset, H. H. Gutbrod, W. G. Meyer, A. M. Poskanzer, A. Sandoval, R. Stock, and G. D. Westfall, Phys. Rev. C 16, 629 (1977).

[13]L. Oliveira, Ph.D. thesis, University of California, Lawrence Berkeley Laboratory Report No. 8561, 1979 (unpublished).

[14]S. Das Gupta, Phys. Rev. Lett. 41, 1450 (1978).

[15]S. Das Gupta and C. S. Lam, Phys. Rev. C 20, 1192 (1979).

[16]E. Forest, S. Das Gupta, and C. S. Lam, Phys. Rev. C 21, 1989 (1980).

[17]W. D. Myers, Nucl. Phys. A296, 177 (1978).

[18]J. Gosset, J. I. Kapusta, and G. D. Westfall, Phys. Rev. C 18, 844 (1978).

[19]C. M. Ko and P. J. Siemens, Nucl. Phys. A367, 496 (1981).

[20]J. Hufner and J. Knoll, Nucl. Phys. A290, 460 (1977).

[21]M. M. Sternheim and R. R. Silbar, Phys. Rev. D 6, 3117 (1972).

[22]R. L. Kelly, C. P. Horne, M. J. Losty, A. Rittenberg, T. Shimada, T. G. Tripper, C. G. Wohl, G. P. Yost, N. Barash-Schmidt, C. Bricman, C. Dionisi, M. Mazzucato, L. Montanet, R. L. Crawford, M. Roos, and B. Armstrong, Rev. Mod. Phys. 52, no. 2 part II (1980).

[23]P. Hecking, Phys. Lett. B103, 401 (1981).

[24]M. I. Sobel, P. J. Siemens, J. P. Bondorf, and H. A. Bethe, Nucl. Phys. A251, 502 (1975).

[25]H. H. Heckman, D. E. Greiner, P. J. Lindstrom, and H. Shwe, Phys. Rev. C 17, 1735 (1978).

[26]El-Bakry, Ph.D. thesis, Cairo University, 1981 (unpublished).

[27]J. W. Negele and K. Yazaki, Phys. Rev. Lett. 47, 71 (1981).

[28]K. Nakai, J. Chiba, I. Tanihata, M. Sasao, H. Bowman, S. Nagamiya, and J. O. Rasmussen, Phys. Rev. C 20, 2210 (1979).

[29]K. L. Wolf, H. H. Gutbrod, W. G. Meyer, A. M. Poskanzer, A. Sandoval, R. Stock, J. Gosset, C. H. King, G. King, Nguyen Van Sen, and G. D. Westfall, Phys. Rev. Lett. 42, 1448 (1979).

[30]G. Bertsch, private communications to collaborators.

[31]J. P. Sullivan, J. A. Bistirlich, H. R. Bowman, R. Bossingham, T. Buttke, K. M. Crowe, K. A. Frankel, C. J. Martoff, J. Miller, D. L. Murphy, J. O. Rasmussen, W. A. Zajc, O. Hashimoto, M. Koike, J. Peter, W. Benenson, G. M. Crawley, E. Kashy, and J. A. Nolen, Jr., Phys. Rev. C 25, 1499 (1982).

[32]P. J. Siemens and J. O. Rasmussen, Phys. Rev. Lett. 42, 880 (1979).

[33]S. Nagamiya, M.-C. Lemaire, E. Moeller, S. Schnetzer, G. Shapiro, H. Steiner, and I. Tanihata, Phys. Rev. C 24, 971 (1981).

This report was done with support from the Department of Energy. Any conclusions or opinions expressed in this report represent solely those of the author(s) and not necessarily those of The Regents of the University of California, the Lawrence Berkeley Laboratory or the Department of Energy.

Reference to a company or product name does not imply approval or recommendation of the product by the University of California or the U.S. Department of Energy to the exclusion of others that may be suitable.

TECHNICAL INFORMATION DEPARTMENT
LAWRENCE BERKELEY LABORATORY
UNIVERSITY OF CALIFORNIA
BERKELEY, CALIFORNIA 94720